Spin orbit correlations and the structure of the nucleon

H. Avakian[1][*], B. Parsamyan[2][**] and A. Prokudin[3][1][***]

[1] *Thomas Jefferson National Accelerator Facility - Newport News, Virginia 23606, USA*
[2] *CERN - CH-1211 Geneva 23, Switzerland*
[3] *Penn State Berks - Reading, Pennsylvania 19610, USA*

Summary. — Extensive experimental measurements of spin and azimuthal asymmetries in various processes have stimulated theoretical interest and progress in the studies of the nucleon structure. The interpretation of experimental data in terms of parton distribution functions, generalized to describe transverse momentum and spatial parton distributions, is one of the main remaining challenges of modern nuclear physics. These new parton distribution and fragmentation functions encode the motion and the position of partons and are often referred to as three-dimensional distributions describing the three-dimensional (3D) structure of the nucleon. Understanding of the production mechanism and performing phenomenological studies compatible with factorization theorems using minimal model assumptions are goals of the analysis of the experimental data. HERMES and COMPASS Collaborations and experiments at Jefferson Lab have collected a wealth of polarized and unpolarized Semi-Inclusive Deep Inelastic Scattering (SIDIS) data. These data play a crucial role in current understanding of nucleon spin phenomena as they cover a broad kinematical range. The Jefferson Lab 12 GeV upgrade data on polarized and unpolarized SIDIS will have a remarkably higher precision at large parton fractional momentum x compared to the existing data. We argue that both experimental and phenomenological communities will benefit from the development of a comprehensive extraction framework that will facilitate the extraction of the 3D nucleon structure, help understand various assumptions in extraction and data analysis, help to insure the model independence of the experimental data and validate the extracted functions. In this review we present the latest developments in the field of the spin asymmetries with emphasis on observables beyond the leading twist in SIDIS, indispensable for studies of the complex 3D nucleon structure, and discuss different components involved in precision extraction of the 3D partonic distribution and fragmentation functions.

(*) E-mail: avakian@jlab.org
(**) E-mail: bakur.parsamyan@cern.ch
(***) E-mail: prokudin@jlab.org

1. – Introduction

Quantum chromodynamics (QCD) is an established theory of strong interactions between quarks and gluons, the fundamental building blocks of the proton and the neutron. The experimental studies in the last several decades of Deep Inelastic Scattering (DIS) and Drell-Yan (DY) processes were pivotal in our tests of QCD, in explaining the behavior of the strong coupling constant, and the collinear parton densities. The spin structure of the hadrons always poses additional complications, continuously challenging the theory, as quark-gluon interactions, and their correlations with the spin of partons and hadrons, are very significant and often are not easily understood in a simple picture of static partons in the nucleon. Relatively recent experimental explorations of the spin-dependent observables in SIDIS, DY, e^+e^-, and hadron-hadron scattering spurred extensive theoretical and phenomenological studies opening a new era of exploration of the 3D structure of the nucleon. Together with rapid advances of precision of lattice QCD calculations and detailed predictions from theory and phenomenology, new precise experimental data are needed. In the process of moving from "testing QCD" to actually understanding it in its full complexity, SIDIS has emerged as a powerful tool to probe the dynamics of strong interactions. The transition from simple, one-dimensional description using collinear parton distributions that depend on nucleon's longitudinal momentum fraction, x, to more complex nucleon picture with interacting and orbiting quarks, leads to a generalization of partonic distributions, to include also the transverse parton momentum, $\mathbf{k}_T$, and to introduction of Transverse Momentum Dependent (TMD) partonic distributions, see fig. 1. SIDIS provides access to TMD partonic distributions through measurements of spin and azimuthal asymmetries. Studies of spin-azimuthal asymmetries in semi-inclusive and hard exclusive production of photons and hadrons have been widely recognized as key objectives of the Jefferson Lab 12 GeV [1,2] upgrade and one of the driving forces for the future Electron Ion Collider [3-7].

SIDIS $(\ell(k) + N(P) \rightarrow \ell'(k') + h(P_h) + X(P_X))$ reaction is such that a beam lepton ℓ with the 4-momenta k, scatters off of a target nucleon, N, with four momentum P, and the scattered lepton ℓ' with four momentum k' is detected along with a single hadron, h with four momentum P_h; all other produced particles in the final state, X, are not detected, see fig. 2. Assuming a single photon exchange, the SIDIS cross-section can be decomposed into a sum of various azimuthal modulations coupled to corresponding
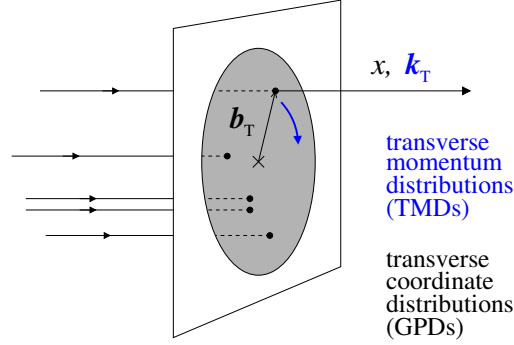
Fig. 1. – Three-dimensional structure of a fast-moving nucleon. The distribution of partons (quarks, gluons) is characterized by the longitudinal momentum fraction x and the transverse spatial coordinate $\boldsymbol{b}_T$ through the impact parameter GPDs [8]. In addition, the partons are distributed over transverse momenta $\mathbf{k}_T$, reflecting their orbital motion and interactions in the system (TMDs) [9, 10]. Polarization distorts both the spatial and momentum distributions. Figure from refs. [6, 4].
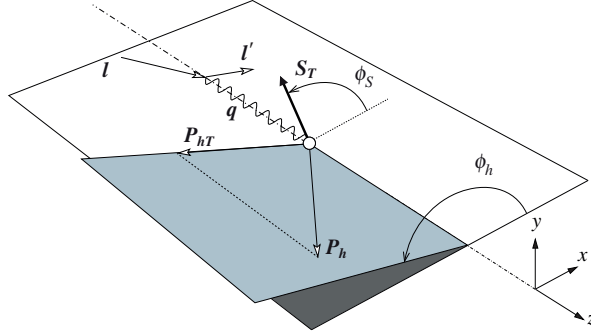

Fig. 2. – SIDIS kinematical plane with definitions of transverse variables.

structure functions. The SIDIS cross-section has following form [9-11]:

$$
(1) \quad \frac{\mathrm{d}\sigma}{\mathrm{d}x\,\mathrm{d}y\,\mathrm{d}z\,\mathrm{d}P_{hT}^2\mathrm{d}\phi_h\mathrm{d}\phi_S} = \hat{\sigma}_U\Big\{1 + \varepsilon A_{UU}^{\cos 2\phi_h}\cos 2\phi_h + \sqrt{2\varepsilon(1+\varepsilon)}A_{UU}^{\cos\phi_h}\cos\phi_h
$$

$$
+\lambda_\ell\sqrt{2\varepsilon(1-\varepsilon)}A_{LU}^{\sin\phi_h}\sin\phi_h
$$

$$
+S_\parallel\Big[\sqrt{2\varepsilon(1+\varepsilon)}A_{UL}^{\sin\phi_h}\sin\phi_h + \varepsilon A_{UL}^{\sin 2\phi_h}\sin 2\phi_h\Big]
$$

$$
+S_\parallel\lambda_\ell\Big[\sqrt{1-\varepsilon^2}A_{LL} + \sqrt{2\varepsilon(1-\varepsilon)}A_{LL}^{\cos\phi_h}\cos\phi_h\Big]
$$

$$
+S_\perp\Big[A_{UT}^{\sin(\phi_h-\phi_S)}\sin(\phi_h-\phi_S)+\varepsilon A_{UT}^{\sin(\phi_h+\phi_S)}\sin(\phi_h + \phi_S)+\varepsilon A_{UT}^{\sin(3\phi_h-\phi_S)}\sin(3\phi_h-\phi_S)
$$

$$
+\sqrt{2\varepsilon(1+\varepsilon)}A_{UT}^{\sin\phi_S}\sin\phi_S + \sqrt{2\varepsilon(1+\varepsilon)}A_{UT}^{\sin(2\phi_h-\phi_S)}\sin(2\phi_h - \phi_S)\Big]
$$

$$
+S_\perp\lambda_\ell\Big[\sqrt{(1-\varepsilon^2)}A_{LT}^{\cos(\phi_h-\phi_S)}\cos(\phi_h - \phi_S)
$$

$$
+\sqrt{2\varepsilon(1-\varepsilon)}A_{LT}^{\cos\phi_S}\cos\phi_S + \sqrt{2\varepsilon(1-\varepsilon)}A_{LT}^{\cos(2\phi_h-\phi_S)}\cos(2\phi_h - \phi_S)\Big]\Big\},
$$

where asymmetries $A_{\cdots}^{\cdots}$ [11] depend on the kinematical variables x, Q^2, z, P_{hT} and correspond to azimuthal modulations of the cross-section in the azimuthal angle ϕ_S of transverse spin and/or azimuthal angle ϕ_h of the produced hadron, both defined in the $\gamma^* N$ c.m. frame (see fig. 2). The first and second subscripts denote, respectively, the lepton and target nucleon polarizations, while the superscript indicates the corresponding azimuthal modulation. Asymmetries are defined as ratios of the corresponding polarized structure functions $F_{\cdots}^{\cdots}$ and unpolarized structure function F_{UU}. The unpolarized structure function, F_{UU}, or more precisely the combination of structure functions corresponding to transverse and longitudinal polarization of the virtual photon, $F_{UU,T} + \varepsilon F_{UU,L}$, is included in the definition of $\hat{\sigma}_U$. We use the usual SIDIS kinematical variables x, y, and z defined as $x = Q^2/2(P \cdot q)$, $y = (P \cdot q)/(P \cdot k)$, $z = (P_h \cdot P)/(P \cdot q)$, where $Q^2 = -q^2 = -(k - k')^2$ is the negative four-momentum squared of the virtual photon, and P_{hT} is the transverse momentum of the detected hadron. The ratio ε of the longitudinal and transverse photon flux is given by $\varepsilon = \frac{1-y-\gamma^2 y^2/4}{1-y+y^2/2+\gamma^2 y^2/4}$, where $\gamma = 2Mx/Q$, and M is the mass of the nucleon.

In the kinematical region, where the TMD description of SIDIS is appropriate, namely in the beam fragmentation region, $P_{hT}/z \ll Q$, the transverse momentum of the produced hadron P_{hT} is generated by intrinsic momenta of the parton in the nucleon $\mathbf{k}_T$ and the transverse momentum of the produced hadron with respect to the fragmenting parton $\mathbf{p}_T$, such that the structure functions become convolutions of the TMD parton distribution functions (PDFs), and TMD fragmentation functions (FFs). The convolution integral, for a given combination of TMD PDF f and FF D reads [11]

$$(2) \qquad \mathcal{C}[wfD] =$$

$$x \sum_q e_q^2 \int \mathrm{d}^2 \mathbf{k}_T \, d^2 \mathbf{p}_T \delta^{(2)}(\mathbf{p}_T + z\mathbf{k}_T - \mathbf{P}_{hT}) w(\mathbf{k}_T, \mathbf{p}_T) f^q(x, k_T^2) D^q(z, P_{hT}^2),$$

where w is a kinematical factor, and the sum goes over all flavors of quarks and antiquarks. The well-known SIDIS structure functions $F_{UU,T}$ and F_{LL} will be, thus, described by convolutions of f_1 and g_1 TMD PDFs and D_1 the unpolarized TMD fragmentation function, with $F_{UU,T} = \mathcal{C}[f_1 D_1]$, $F_{LL} = \mathcal{C}[g_1 D_1]$. The full list of TMD PDFs accessible in SIDIS is given in table I. The TMDs depend on the polarization state of the quark (rows) and polarization state of the nucleon (columns). The corresponding tables for TMD FFs can be found in review [12].

Apart from the Q^2 dependence of the elementary lepton-quark cross-section $\propto Q^{-4}$, some structure functions appear in the cross-section either unsuppressed or suppressed by an additional power of the hard scale Q. Accordingly, the structure functions can be classified as subleading-twist Q^{-1} (twist-3) effects and leading-twist Q^0 (twist-2) effects [13]. Higher-twist structure functions will include convolutions of higher-twist TMD functions. Several collinear higher-twist distributions, like g_T, for instance, are accessible in DIS where collinear factorization applies, and bear physics of significant interest [14]. While the definition of twist itself is problematic [15,16] in the TMD formalism, one can characterize twist expansion rigorously using the collinear operator product expansion (OPE) of the scattering amplitude, such that the twist classifies operators and isolates the leading contributions, at twist-2, from the subleading- higher-twist contributions, power suppressed as $Q^{2-\mathrm{twist}}$. The leading and higher-twist non-perturbative functions describe various spin-spin and spin-orbit correlations as the corresponding operators include additional gluon and/or quark fields in the matrix element.

TABLE I. – *Tables for leading (left) and subleading (right) TMDs, with columns indicating the quark, and rows the nucleon polarization* [10, 11, 17].

quark / nucleon	U	L	T	quark / nucleon	U	L	T
U	f_1		$h_1^\perp$	U	$f_\perp, e$	$g^\perp$	h
L		g_{1L}	$h_{1L}^\perp$	L	$f_L^\perp$	$g_L^\perp$	h_L, e_L
T	$f_{1T}^\perp$	g_{1T}	$h_1, h_{1T}^\perp$	T	$f_T, f_T^\perp, e_T^\perp$	$g_T, g_T^\perp, e_T$	$h_T, h_T^\perp$

Many structure functions involve transversely polarized quarks. For example the $F_{UU}^{\cos 2\phi}$, at leading twist is interpreted as a convolution of Boer-Mulders distribution function, $h_1^\perp$ that encodes the correlation between the transverse motion of a quark and its own transverse spin [18], and the Collins fragmentation function, $H_1^\perp$ [19], that describes fragmentation of transversely polarized quarks into an unpolarized hadron.

Measurements of flavor asymmetries in the sea quark distributions performed in DY experiments indicate very significant non-perturbative effects at large Bjorken-x, where the valence quarks are relevant [20]. In perturbative QCD $q\bar{q}$ pairs are created from the gluon splitting. Since the masses of u and d quarks are small, the gluon splitting is not expected to generate quark flavor asymmetries. Older measurements by NMC [21] indicated that integrated $\bar{d}$ is more than integrated $\bar{u}$. The measurements by the E866 Collaboration [22], and more recently by SeaQuest [23] suggest that $\bar{d}$ is significantly larger than $\bar{u}$ in the full accessible x-range. The non-perturbative $q\bar{q}$ pairs are also correlated with spins and play a crucial role in spin orbit correlations, and in particular, single-spin asymmetries measured by various experiments in last few decades.

The interpretation of the leading-twist structure functions in terms of convolutions of TMD distributions rises from factorization theorems, see ref. [24] and references therein. Subleading structure functions require a proof of validity of TMD factorization at higher twist and the proof is not yet available, however studies of subleading twists are also important, as they may affect significantly the extraction of leading-twist moments, as the radiative effects, and complicated acceptances of wide-angle spectrometers may introduce cross-talk between different azimuthal moments in the spin-dependent and spin-independent moments. For instance, $\cos\phi$ modulation asymmetry known as the Cahn effect [25], is significant ($\sim$ 20–30%) and dominating in the $P_{hT} \sim 1\,\text{GeV}$ range, even though it is suppressed by P_{hT}/Q with respect to leading-twist asymmetries. Additional contributions to $\cos\phi$ and $\cos 2\phi$ moments coming from processes when the final meson is produced at short distances via hard-gluon exchange [26] may also be significant in the kinematic regime where the ejected meson carries most of the virtual photon momentum (z approaching 1).

Even though we do not have enough direct information about higher-twist TMDs from experimental data, one may hope that the quark models give estimates for higher-twist TMDs, and whether the modeling can be useful for phenomenological studies. The applicability of quark models to TMDs beyond leading twist still remains debatable, however the additional information on higher-twist TMDs from models may become very important for phenomenology and for experimental event generators.

The projected accuracy of Jefferson lab 12 GeV upgrade data for the ϕ_h-dependent multiplicities is comparable to effects arising from the fine structure constant, $\alpha_{em} \approx$

1/137, and therefore neglecting electromagnetic corrections of the order $\mathcal{O}(\alpha_{em})$ may lead to significant mis-interpretation of the data. Extension and further development of the theoretical and computational approaches to higher-order QED effects for electron scattering is an outstanding problem for the upcoming physics analysis effort at Jefferson Lab. Disentangling the cross-section $\sigma_0^{ehX}(x, y, z, P_{hT}, \phi_h, \phi_S)$ from measurements is a very important task, complicated by the fact that radiative corrections to cross-section introduce significant corrections to contributions and may introduce additional azimuthal moments in the cross-section [27, 28]

$$(3) \qquad \sigma_{\mathrm{Rad}}^{ehX}(x, y, z, P_{hT}, \phi, \phi_S) \rightarrow$$

$$\sigma_0^{ehX}(x, y, z, P_{hT}, \phi_h, \phi_S) \times R(x, y, z, P_{hT}, \phi_h) + R_A(x, y, z, P_{hT}, \phi_h, \phi_S).$$

Studies of the model dependence in Radiative Correction (RC) calculations in the full kinematical region will be important for precision studies of underlying 3D PDFs from Jefferson Lab12 to EIC and require simultaneous extraction of all moments to account for various correlations. The methodology for accounting for radiative effects in SIDIS is currently a generalized version tested for DIS studies: typically one uses RADGEN generator [29] combined with different full event generators, like PYTHIA, LEPTO, PEPSI [30-32]. This approach, while providing some estimates for RC, is not fully consistent for SIDIS, as RADGEN itself contains only DIS structure functions, and the LUND model based generators at the moment do not include spin-orbit correlations in the fragmentation. Precision studies of azimuthal moments in SIDIS will require a completely new methodology to account for RC effects in SIDIS, taking as input a set of realistic structure functions that describe all relevant moments for specific observables under study. Thus we expect that phenomenological studies will attempt extraction of all azimuthal moments and a full set of TMDs contributing to the SIDIS cross-section for a given configuration of beam and target polarizations.

One of the most important questions about the 3D structure of the nucleon is the transverse momentum dependence of the distribution and fragmentation TMDs and flavor and spin dependence of those shapes. For precision studies of TMDs it is also important to understand the role of medium, and the effects of in medium modifications of TMDs. That is crucial, since both COMPASS and JLab use nuclear targets to study polarization effects. Another important question to address is the role of exclusive processes in studies of SIDIS. In order to extract the underlying functions and thus details of dynamics of quarks and gluons from SIDIS data one also has to have a good understanding of the underlying fragmentation process in which the quark fragments into an observed hadron. Exclusive processes may shed light on the fragmentation process itself.

The structure of this mini-review is the following. After a brief introduction of experimental facilities and important measurements of SIDIS leading-twist observables (sects. **2-3**), we will discuss the higher-twist SIDIS observables (sect. **4**). In sect. **5** we discuss the relevance of different flavors of hadrons in studies of the complex nucleon structure, followed by discussion of some unique possibilities enabled by detection of di-hadron final states in sect. **6**. The final section **7** is devoted to challenges and possible methodology of extraction of non-perturbative partonic distribution and fragmentation functions from the wealth of the experimental data, already available and expected from future measurements at COMPASS and upgraded Jefferson Lab, as well as future Electron Ion Collider.

TABLE II. – *Main characteristics of SIDIS detectors.*

Experiment	Beam	Target	Energy GeV	Lumi	Polarization
HERMES	e^+e^-	H_2, D_2, N, C	27.5	10^{32}, 10^{33}	U/L/T
COMPASS	μ^+	NH_3, ^{6}LiD	160, 200	10^{33}	U/L/T
JLab CLAS	e^-	H_2, D_2, NH_3, ND_3	6, 11	10^{34}–10^{35}	U/L/T
JLab Hall-A	e^-	^{3}He	6, 11	10^{37}	U/L/T
JLab Hall-C	e^-	H_2, D_2	6, 11	10^{38}	U
JLab Solid	e^-	^{3}He, NH_3	6, 11	10^{36}–10^{37}	U/L/T
EIC [33]	e^-	p, d, A	3–$12(e)/20$–$400(p)$	0.5–5.10^{34}	U/L/T

2. – SIDIS experiments

Several experiments worldwide were involved in studies of SIDIS with different hadrons produced. Most of the latest relevant data for studies of spin-orbit correlations was coming from HERMES Collaboration at HERA, COMPASS Collaboration at CERN, and measurements already performed at JLab. As for the near future, a wide spectra of high-precision measurements will be done at JLab12, while COMPASS plans to collect more SIDIS data with transversely polarized deuteron target in 2021 [34]. Major advantages of different setups include gas target from HERMES with fast target spin flip, providing clean target spin asymmetries with no dilution from nuclear target, high-energy muon beam of COMPASS with relatively small radiative corrections, and superior beam polarization at JLab, allowing clean measurements of beam-spin asymmetries. The wider angle coverage of CLAS12 detector allows measurements in a wide range of P_{hT} (up to 1.5 GeV), and Q^2 (up to 10 GeV^2), while the SoLID detect would allow measurements of all kinds of polarization asymmetries at large Bjorken-x with superior precision.

Table II shows the main characteristics of the SIDIS experiments involved in TMD studies. At JLab all 3 halls are involved in 3D structure studies [2] including the HMS and Super HMS at Hall C [35-37], the BigBite and Super BigBite, as well as the SoLID detector at Hall A [38-40], and CLAS12 at Hall B [41, 42]. Several experiments are already approved to study in details the azimuthal modulations in SIDIS for different hadron types, targets, and polarizations in a broad kinematic range [41-44, 39, 36, 38, 40]. The experimental investigation of medium modification of quark fragmentation and spin-orbit correlation will be also extensively pursued at the upgraded Jefferson Lab facility, for which several related experimental proposals already exist [45, 46].

3. – Leading-twist observables

Correlations of quark transverse momenta with their own spin or spin of the parent hadron manifest themselves in different spin-dependent azimuthal moments in the cross-section, generated either by correlations in the distribution of quarks or in the fragmentation process. The most known correlations are often referred to as Sivers type [47] and Collins type [19], respectively, see Review [48]. The involved structure functions factorize into TMD parton distributions and fragmentation functions, and hard parts [49].

The most prominent leading-twist observable is the ϕ_h-integrated cross-section described by the F_{UU} structure function. Experiments, however, prefer to measure the

multiplicities of hadrons, which is the ratio of SIDIS cross-sections for a given type of hadron divided by DIS cross-section in a given bin in x, Q^2 (the advantage is that *e.g.* the scattered lepton acceptance entering in the numerator and denominator cancels). As one can see from eq. (2), in the TMD formalism the final hadron $\mathbf{P}_{hT}$ results from the initial quark $\mathbf{k}_T$ and the fragmenting quark $\mathbf{p}_T$ and up to order $\mathcal{O}(k_T/Q)$ the momentum conservation gives $\mathbf{P}_{hT} = z\mathbf{k}_T + \mathbf{p}_T$. The structure function F_{UU} is given by the convolution integral $\mathcal{C}[f_1 D_1]$

$$(4) \qquad F_{UU}(x,z,P_{hT}) = x \sum_q e_q^2 \int \mathrm{d}^2\mathbf{k}_T \, \mathrm{d}^2\mathbf{p}_T \delta^{(2)}(\mathbf{p}_T + z\mathbf{k}_T - \mathbf{P}_{hT}) f_1^q(x,k_T^2) D_1^q(z,P_{hT}^2).$$

Notice that eq. (4) was initially proposed in the parton model approximation, see for instance [11]. The result of the factorization proof of ref. [24] formally coincides with eq. (4), however the TMD functions have a much more intricate dependence on the scales present in the process. This dependence is governed by the evolution equations and allows to predict the change of the shape of TMDs without using the model assumptions. The complication of implementation of the TMD factorization is the presence [24] of a universal non-perturbative kernel of evolution. This kernel and the non-perturbative shape of TMDs should be extracted from the global fit of low- and high-energy experimental data.

In this review we will consider only the approximate description of TMDs in the non-perturbative region and analytical results that can be obtained using simplified assumptions. In order to resolve the convolution integral of eq. (4), one makes assumptions on the k_T dependence of f_1 and the P_{hT} dependence of D_1 and individuates a set of parameters which would be then extracted in an analysis of multidimensional data on either F_{UU} or multiplicity. For example, a common assumption is the Gaussian ansatz for the transverse momentum dependence of distribution and fragmentation functions [50, 51] which would result in the average P_{hT} given by

$$(5) \qquad \langle P_{hT}(z) \rangle = \frac{\sqrt{\pi}}{2} \sqrt{z^2 \langle k_T^2 \rangle + \langle p_T^2 \rangle},$$

where $\langle k_T^2 \rangle$ and $\langle p_T^2 \rangle$ (GeV^2) are Gaussian widths of the k_T dependence of f_1 and the P_{hT} dependence of D_1.

Collinear PDFs have flavor dependence, thus it is not unexpected that also the transverse momentum dependence may be different for the different flavors [51]. Model calculations of transverse momentum dependence of TMDs [52-55] and lattice QCD results [56,57] suggest that the dependence of the widths of TMDs on the quark polarization and flavor may be significant. It was found, in particular, that the average transverse momentum of antiquarks is considerably larger than that of quarks [58, 59]. The frequently used assumption of factorization of x and k_T (or z and P_{hT}) dependencies [50] may be significantly violated (see fig. 10 of [60]). For instance the predicted average transverse momentum square $\langle k_T^2 \rangle$ of quarks and antiquarks may depend strongly on their longitudinal momentum fraction x within the framework of the chiral quark soliton model.

In the fragmentation process, one would expect [61] that the *dis-favored* fragmentation of a quark into a hadron would be broader in the transverse momentum with respect the *favored* fragmentation (fragmentation of a quark to a hadron that has this type of quark as a valence quark).
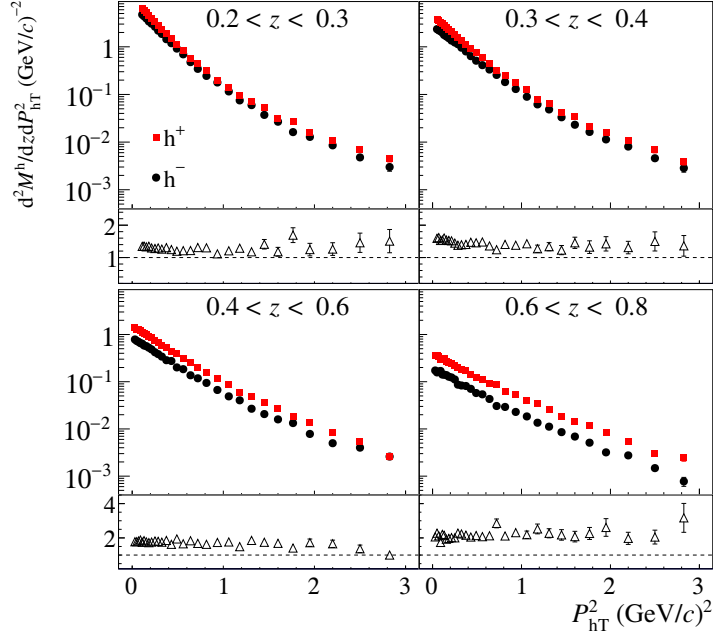
Fig. 3. – Multiplicities of positively (full squares) and negatively (full circles) charged hadrons at COMPASS [65]. Upper panels: multiplicities of charged hadrons as a function of P_{hT} in four z bins at $Q^2 = 9.78$ $(\mathrm{GeV}/c)^2$ and $x = 0.149$. Lower panels: ratio of multiplicities of positively and negatively charged hadrons.

The production of charged pions in SIDIS has been measured from both proton and deuteron targets, using a 5.5 GeV energy electron beam in Hall-C at Jefferson Lab [62]. In the limited $P_{hT}^2 < 0.2$ explored, the P_{hT} dependence from the deuteron was found to be slightly weaker than from the proton. In the context of a simple model this would suggest that transverse momentum distributions may depend on the flavor of quarks. Multiplicities of charged pion and kaon mesons have been measured by HERMES using the electron beam scattering off hydrogen and deuterium targets [63]. Multiplicities of charged hadrons produced in deep inelastic muon scattering off a ^{6}LiD target have been measured at COMPASS [64]. These high-statistics data samples have been used in phenomenological analyses [50, 51, 60] to extract information on the flavor dependence of unpolarized TMD distribution and fragmentation functions. Restricting the ranges of the available data to $Q^2 > 1.69$ $(\mathrm{GeV}/c)^2$, $z < 0.7$ and $0.2\,\mathrm{GeV}/c < P_{hT} < 0.9\,\mathrm{GeV}/c$, the authors of ref. [50] obtained a reasonable description of the experimental data within a Gaussian assumption for TMDs with flavor independent and constant widths, $\langle k_T^2 \rangle$ and $\langle p_T^2 \rangle$. Nevertheless, indications were reported that the favoured fragmentation functions into pions have a smaller average transverse momentum width than unfavoured functions and fragmentation functions into kaons [51], consistent with predictions based on the NJL-jet model [61]. The latest multiplicity measurements at COMPASS [65] shown in fig. 3 indicate that the ratio of counts of positive and negative hadrons increases with z, which can be explained by the fact that, in contrast to $\pi^\pm$, K^+ and p, negative

hadrons K^- and $\bar{p}$ cannot be produced by the favoured fragmentation of nucleon valence quarks. In addition, the ratio tends to decrease with P_{hT} at relatively small z, where the fraction of exclusive events is not essential. The comparison of COMPASS with HERMES and JLab measurements of multiplicities performed in ref. [65] shown in fig. 4 unveils significant differences which could be due to the different Q^2 ranges covered by the experiments and supports findings of studies from ref. [66] indicating that at lower energies the large values of P_{hT} are suppressed due to smaller phase space, in particular at large z. The latter is confirmed by recent COMPASS results obtained for the K^- over K^+ multiplicity ratio at large fraction z of the virtual-photon energy [67].

The origin of the $\cos 2\phi_h$ modulation, $F_{UU}^{\cos 2\phi_h}$, due to the convolution of the Collins fragmentation function $H_1^\perp$, describing fragmentation of transversely polarized quarks, and the Boer-Mulders distribution function $h_1^\perp$, describing distributions of transversely polarized quarks in an unpolarized nucleon, was first discussed by Boer and Mulders in 1998 [18]. The structure function reads

$$(6) \qquad F_{UU}^{\cos 2\phi_h}(x, z, P_{hT}) = \mathcal{C}\left[\frac{2(\hat{\boldsymbol{h}} \cdot \mathbf{k}_T)(\hat{\boldsymbol{h}} \cdot \mathbf{p}_T) - (\mathbf{p}_T \cdot \mathbf{k}_T)}{zM_N m_h} h_1^\perp(x, k_T^2) H_1^\perp(z, P_{hT}^2)\right].$$

In addition to this, when the intrinsic transverse momenta $\mathbf{k}_T$ of quarks inside the nucleon are taken into account a subleading-twist Q^{-2} (twist-4) contribution to the $\cos 2\phi$ amplitude originates from the Cahn effect [25] (kinematic correction at the level of the elastic quark-lepton cross-section). This contribution is expected to dominate at small x. Measurements of the $\cos 2\phi$ moments have been published by different experiments. Significant positive $\cos 2\phi$ amplitudes for both positively and negatively charged hadrons were measured at COMPASS [67]. At HERMES [69], positive $\cos 2\phi$ amplitudes are extracted for negatively charged pions, while for positively charged pions the moments are compatible with zero, but tend to be negative in some kinematic regions. In all the cases, the amplitudes of the cosine modulations show strong kinematic dependencies.
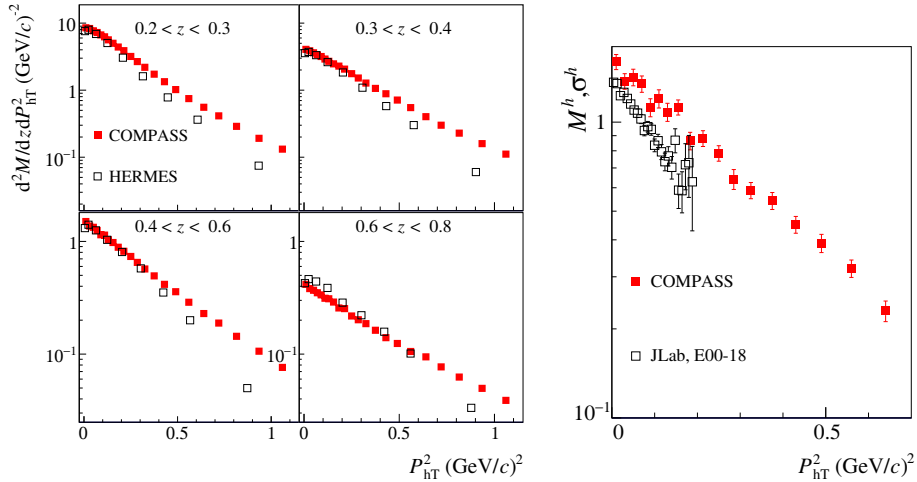

Fig. 4. – Comparison of multiplicities of positively charged hadrons at COMPASS [65] and HERMES [63] (left panel) and at COMPASS [65] and JLab [68] (right panel).

Comparisons between COMPASS and HERMES $\cos 2\phi$ modulations for hadrons in the almost overlapping kinematic region ($0.02 < x < 0.13$, $\langle Q^2 \rangle \simeq 4$ (GeV/c)^2 of COMPASS and $0.023 < x < 0.145$, $\langle Q^2 \rangle \simeq 2$ (GeV/c)^2 of HERMES) require point-to-point correction for the so-called depolarization factor $D(y) = \epsilon$ (the ratio of the longitudinal to transverse virtual photon flux). There is some tension in the z dependence between the two experiments in the $\cos 2\phi$ modulation of positive hadrons (that show the same behaviour but have an off-set of about 0.05). For a detailed comparison between results of different experiments and between results and theoretical models, a full differential analysis using the complete multi-dimensional information is needed [70].

The first observation of a Single Spin Asymmetry (SSA) in semi-inclusive DIS pion electroproduction was made by HERMES [71]. The main goal of the original measurements was to access the distributions of transversely polarized quark in the longitudinally polarized nucleon, $h_{1L}^{\perp}$. The physics of $F_{UL}^{\sin 2\phi}$, which involves the Collins fragmentation function $H_1^{\perp}$ and Mulders distribution function $h_{1L}^{\perp}$, was first discussed by Kotzinian and Mulders in 1996 [10, 9, 72].

$$(7) \qquad F_{UL}^{\sin 2\phi_h}(x, z, P_{hT}) = \mathcal{C}\left[\frac{2(\hat{\boldsymbol{h}} \cdot \mathbf{k}_T)(\hat{\boldsymbol{h}} \cdot \mathbf{p}_T) - (\mathbf{p}_T \cdot \mathbf{k}_T)}{zM_N m_h} h_{1L}^{\perp}(x, k_T^2) H_1^{\perp}(z, P_{hT}^2)\right].$$

The same distribution function is accessible, in particular, in double polarized Drell-Yan, where it gives rise to the $\cos 2\phi$ azimuthal moment in the cross-section [73]. The behavior of the Mulders distribution function was subsequently studied in many models, including large-x [74] and large N_c [75] limits of QCD. Model calculations of Boer-Mulders functions, phenomenological analysis and predictions for JLab measurements of the $\cos 2\phi$ azimuthal moment were given in ref. [76].

Measurements of the $\sin 2\phi$ SSA [72] allow the study of the Collins effect with no contamination from other mechanisms. Measurement of the $\sin 2\phi$ moment of F_{UL} by HERMES [71] appeared to be consistent with zero. A measurably large asymmetry has been predicted only at large x ($x > 0.2$), a region well-covered by JLab [77]. The existing data indeed indicates that at large x the F_{UL} may be significant [78-80]. In fig. 5 the latest COMPASS measurements [79, 80] are compared with $D(y)$-rescaled HERMES points [71] and model predictions for COMPASS kinematics [81].
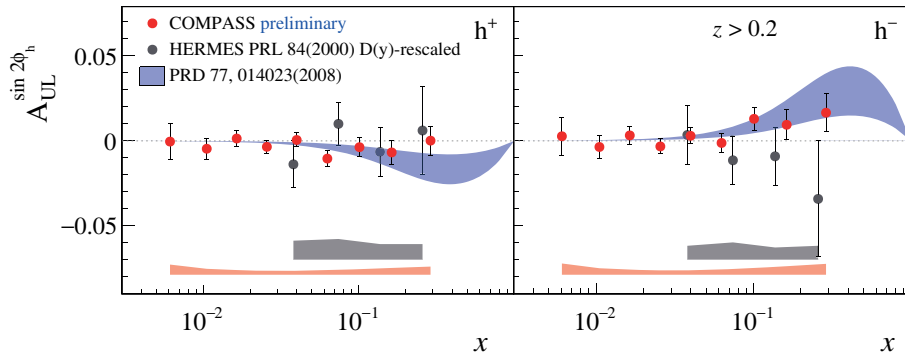

Fig. 5. – The $A_{UL}^{\sin(2\phi_h)}$ results obtained by HERMES [71] and preliminary results by COMPASS [79, 80] and available model predictions [81].
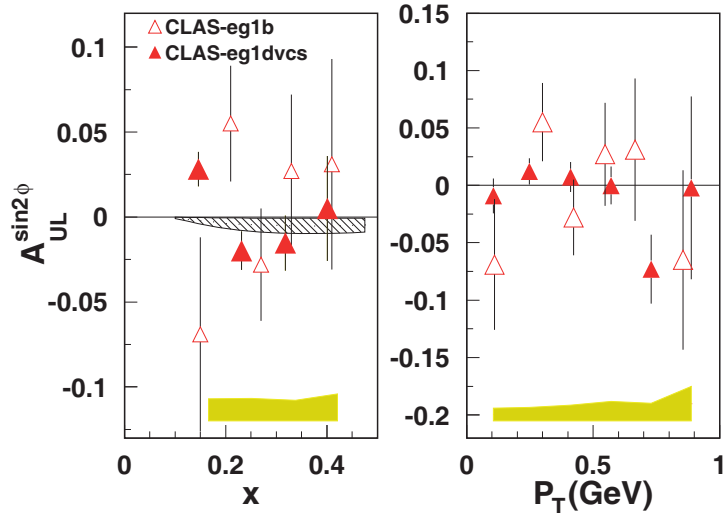
Fig. 6. – The $\sin 2\phi_h$ moments for A_{UL} plotted *versus* x (left) and $\mathbf{P}_{hT}$ (right) [83] compared to previous CLAS measurements [78] and theory predictions (gray band) [81]. The error bars represent the statistical uncertainties, whereas the yellow bands represent the total experimental systematic uncertainties.

Due to the opposite sign of the Collins fragmentation functions for the favored and disfavored hadrons, all kinds of SSAs originating from the Collins mechanism are in principle expected to be suppressed for π^0-production. The latest data from CLAS Collaboration [83] is consistent with previous measurements [78] indicating that the $\sin 2\phi$ target spin-dependent moment, which is expected to depend on the Collins fragmentation function, is much smaller for π^0 than for charged pions, fig. 6.

Large $\sin\phi$ SSA measurements by HERMES [71] spawned a number of additional measurements of SSAs and DSAs (Double-Spin Asymmetries) using polarized hydrogen and deuterium targets [84, 85]. Most prominent are the Collins and Sivers asymmetries. With an unpolarised beam and a transversely polarised target one can get access to the structure function $F_{UT}^{\sin(\phi+\phi_S)}(x, z, P_{hT}, Q^2)$. The latter can be written as a convolution of $h_1(x, k_T, Q^2)$ and $H_1^\perp(z, P_{hT}, Q^2)$, integrated over the transverse momentum of the initial, k_T, and fragmenting, P_{hT}, partons, providing access to distributions of transversely polarized quarks, also known as "transversity" TMD and the Collins fragmentation function

$$(8) \qquad F_{UT}^{\sin(\phi_h+\phi_S)}(x, z, P_{hT}) = \mathcal{C}\left[\frac{\hat{\boldsymbol{h}} \cdot \mathbf{P}_T}{zm_h} h_1(x, k_T^2) H_1^\perp(z, P_{hT}^2)\right].$$

The Collins asymmetries were measured by HERMES [86] with proton target and by COMPASS with deuteron [87-89] and proton targets [90, 91]. The Collins asymmetry on deuteron was found to be small and compatible with zero within the uncertainties, while on proton it has a strong x dependence, *i.e.* compatible with zero in the small x region accessible at COMPASS it increases up to 0.05 in the valence quark region. The asymmetry exhibits a mirror symmetry (similar amplitude, but opposite sign) with
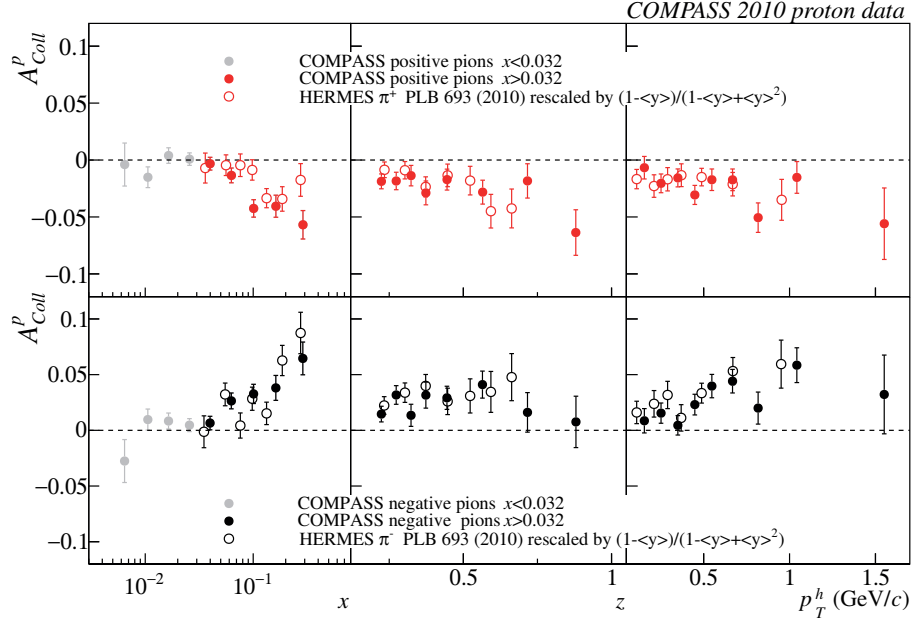
Fig. 7. – Collins asymmetries, $A_{UT}^{\sin(\phi_h+\phi_S)}$, for positive and negative pion production on proton measured at COMPASS [91] requiring $x > 0.032$ (filled circles) are compared with HERMES proton results [86] (empty circles).

respect to the hadron charge, which is attributed to the same size and opposite sign of the favoured and unfavoured Collins FFs. In fig. 7 COMPASS and HERMES proton Collins SSA results for positive and negative pion productions are compared. The asymmetries are found to be in agreement, which is a non-obvious result, taking into account that in the valence region the Q^2 value at COMPASS is as much as two to three times larger compared to that of HERMES. Measurements of Collins asymmetries by HERMES [86] and COMPASS [90, 91] combined with the Belle [92] $e^+e^- \to \pi^+\pi^-$ data are used in global fits allowing to extract the transversity distribution, see $e.g.$ ref. [93]. In 2021 COMPASS is planning to perform one year of semi-inclusive DIS data taking with a transversely polarised deuteron target [34]. This measurement will allow to considerably improve the knowledge on d-quark transversity distribution.

The study of the Sivers effect, describing correlations between the transverse polarization of the nucleon and its constituent (unpolarized) parton's transverse momentum, has been the topic of a great deal of experimental, phenomenological and theoretical effort in recent years. The asymmetry is related to the Sivers TMD PDF ($f_{1T}^\perp(x, k_T^2)$) convoluted with ordinary fragmentation function ($D_1(z, P_{hT}^2)$), the corresponding structure function reads

$$(9) \qquad F_{UT}^{\sin(\phi_h-\phi_S)}(x, z, P_{hT}) = \mathcal{C}\left[-\frac{\hat{\boldsymbol{h}} \cdot \mathbf{k}_T}{M_N} f_{1T}^\perp(x, k_T^2) D_1(z, P_{hT}^2)\right].$$

The most exciting feature, predicted for the Sivers function, is that it is expected to have opposite sign when measured in SIDIS on the one hand, and in DY or W/Z-boson
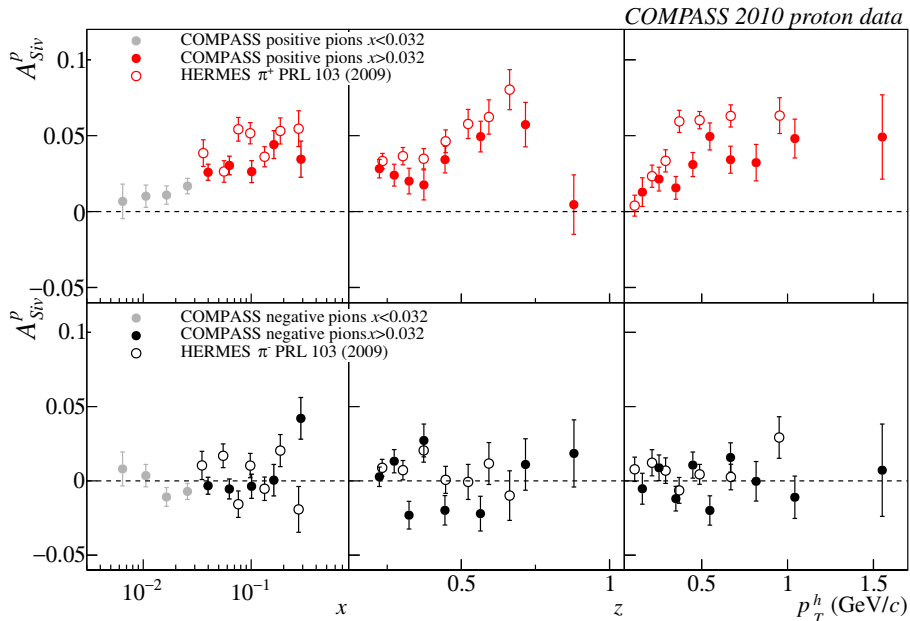
Fig. 8. – Sivers asymmetries, $A_{UT}^{\sin(\phi_h - \phi_S)}$, for positive and negative pion production on proton measured at COMPASS [91] requiring $x > 0.032$ (filled circles) are compared with HERMES proton results [102] (empty circles).

production on the other [94, 95]

$$(10) \qquad \left(f_{1T}^{\perp}\right)_{\text{SIDIS}} = -\left(f_{1T}^{\perp}\right)_{\text{DY}}.$$

The Sivers SSAs for proton and deuteron targets have been published by HER-MES [96, 86] and COMPASS [87-89, 91, 97-100], which provided the first, direct indication of significant interference terms beyond the simple s-wave ($L_z = 0$) picture. The asymmetries become larger with increasing x, suggesting that spin-orbit correlations are significant only in the region of large x ($x > 0.01$), where the valence quarks or non-perturbative sea are relevant [20]. In addition to the classical approach, COMPASS has recently measured also the P_T/zM-weighted Sivers asymmetries accessing directly the first moments of the Sivers functions for u_v and d_v quarks [101].

From the comparison of HERMES [102] and COMPASS [91] proton results in the overlapping kinematic region, unlike the Collins asymmetry, the Sivers effect at HER-MES was found to be somewhat larger compared to that measured at COMPASS (see fig. 8). This observation may hint to the influence of TMD evolution effects. Present models predict for increasing Q^2 a mild dependence of the Sivers asymmetry when the parton model approximation and DGLAP evolution is used and a strong or weak decrease for different TMD evolution schemes, see for instance refs. [103-105]. There is no theoretically compelling argument to use DGLAP evolution for TMDs, only the small-b expansion [24] of TMDs may be related to collinear functions that obey DGLAP evolution. TMD evolution [24, 106] should be quite different from DGLAP. COMPASS recently performed the first multi-differential analysis of the transverse-spin-dependent
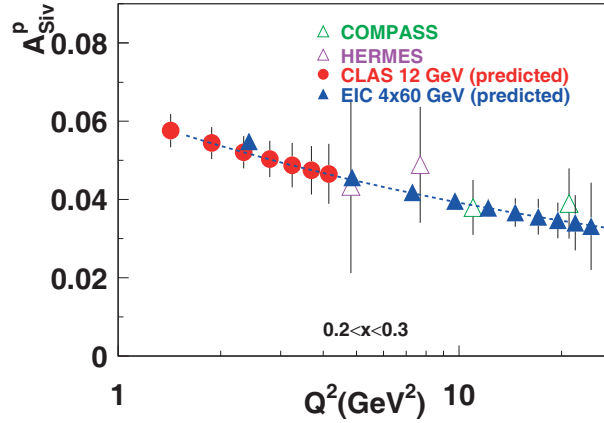
Fig. 9. – Projections for CLAS12 measurements of the Q^2 dependence of the Sivers asymmetry for $ep \rightarrow e'\pi^+X$, compared to HERMES, COMPASS and future EIC measurements.

asymmetries extracting them from SIDIS data at four-five different hard scales [107-109]. Extracted Q^2 dependences of the Sivers SSAs in different bins of x were fitted with a linear decreasing function and a constant with a slight statistical preference for the former case. Evolution properties of TMDs and in particular the Sivers TMD, were predicted to be very different from regular PDFs [110]. Studies of evolution of Sivers TMD require precision measurements in different ranges of Q^2. Projections for the Q^2 dependence of the Sivers effect expected from CLAS12 are shown in fig. 9. The asymmetry, however, like other observables which are constructed by taking ratios, is not an ideal ground for the study of TMD evolution effects, as it has additional modulations coming from the unpolarized part, making interpretation more complicated. Due to the partial cancellation of evolution effects in the numerator and the denominator, the asymmetries themselves may exhibit only a weak Q^2 dependence. It was suggested that more effort should be made towards measuring properly normalized SIDIS and e^+e^-, and Drell-Yan cross-sections (both unpolarized and polarized).

The first measurement of the Sivers effect in W and Z boson production in $p^\uparrow p \rightarrow W^\pm/Z^0 X$ reactions at RHIC was reported by the STAR Collaboration [111], while COMPASS has recently published first ever results for Sivers asymmetry measured in the pion-induced Drell-Yan lepton pair production off a transversely polarized proton [112,113,80], see fig. 10. Both measurements were found to be consistent with the hypothesis of a predicted change of sign for the Sivers function, but the accuracy was not enough to give a conclusive answer. Soon more precise data is expected to come from both experiments.

The Sivers asymmetry for π^+ and π^0 productions in SIDIS appeared to be very close to each other (see fig. 11), a feature showing up also for many kinds of higher-twist modulations. Measurements of SSAs at JLab, performed with transversely polarised ^{3}He [114-118], indicate that spin orbit correlations may be significant for certain combinations of spins of quarks and nucleons and transverse momentum of scattered quarks.

The measurements of the SSAs for hadrons produced in the Target Fragmentation Region (TFR) will allow one to study the structure of the nucleon through the fracture functions. These objects, though more complicated than the ordinary PDFs and FFs, will provide important new information. An updated version of the PYTHIA, mPYTHIA was used to look at correlations between different kinematical regions [119]. The Lund string model used in PYTHIA differs from the usual QCD factorized approach that
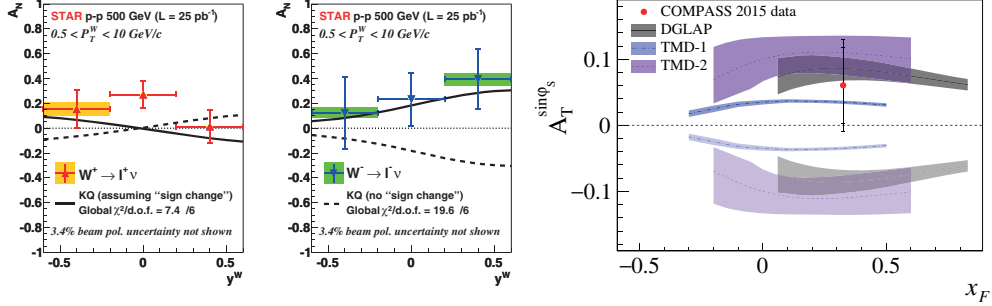
Fig. 10. – Transverse single-spin asymmetry amplitude for W^+ (left panel) and W^- (central panel) from STAR [111] and Sivers asymmetry in Drell-Yan from COMPASS [112] (right panel).
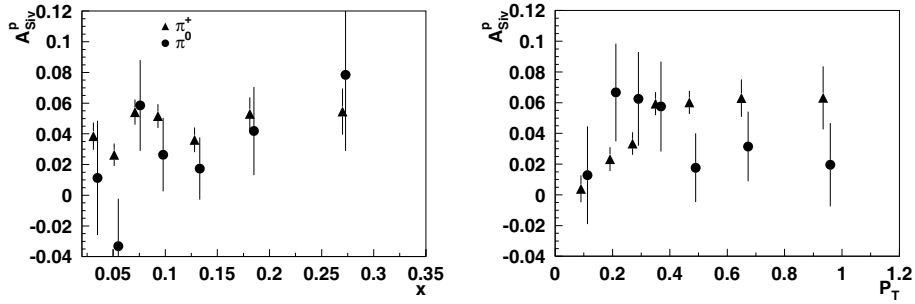

Fig. 11. – Comparison of Sivers asymmetries, $A_{UT}^{\sin(\phi-\phi_S)}$ for neutral and positive pions measured by HERMES Collaboration [102].

describes the hadron production in the Current Fragmentation Region (CFR) with a convolution of PDFs and FFs and in the TFR using two additional independent fracture functions. Studies based on mPYTHIA, accounting only the correlation between the nucleon's transverse polarization and the transverse momentum of the struck quark revealed a sizable signal in the in TFR, comparable in size to that in the CFR (see fig. 12). Experimental measurements of Sivers SSAs in both CFR and TFR will be important to reveal underlying correlations.

There have been many studies dedicated to model calculations of TMDs, see for example [120, 94, 121-124, 76, 125-131, 52, 132, 133]. These models and calculations of asymmetries based on them could play a very important role as a first step of the description of the experimental observations, to give an intuitive way to connect the physical observables to the dynamics of partons, and to provide key inputs to unravel the partonic structure of the nucleon. Models provide a clear way of addressing fundamental questions, such as how the quark spin and its orbital angular momentum contribute to the nucleon spin. Even though models do not contain full QCD dynamics, one may gain insight on full QCD by examining the models. In addition, very exciting results of TMDs have come from lattice QCD calculations [56, 134, 57], indicating, for instance, that spin-orbit correlations could change the transverse momentum distributions of partons. Lattice calculations suggested that transverse momentum distributions depend both on flavor and the spin orientation of quarks (see fig. 13). Measurements of the P_{hT} dependence of the double-spin asymmetry A_1, performed at JLab, with longitudinally polarized NH_3 target [78], suggest
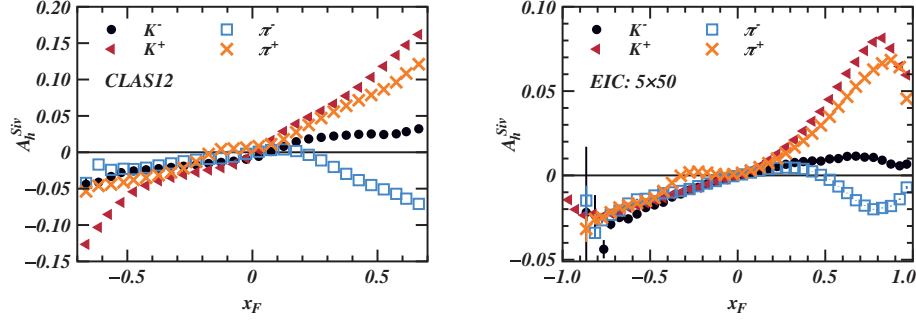
Fig. 12. – Projections for Sivers asymmetry measurements as a function of x_F at JLab (left) and future EIC (right) for positive pion production, using 4 GeV electrons and 60 GeV protons (100 days at $10^{34}\,\mathrm{cm}^{-2}\,\mathrm{sec}^{-1}$) [119].
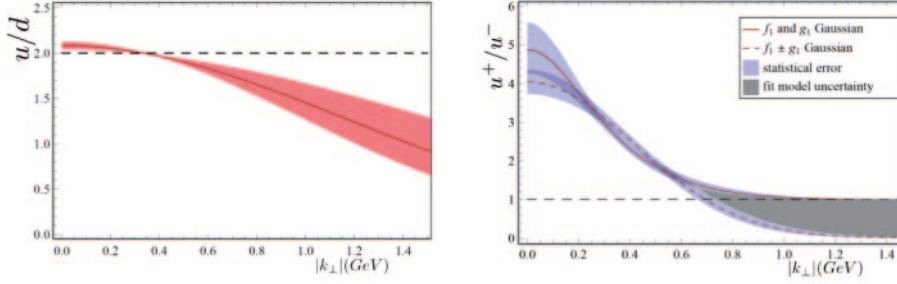

Fig. 13. – Lattice calculations for the k_T dependence of ratios of u/d quark distributions (left) and u^+/u^- distributions (right) [57].
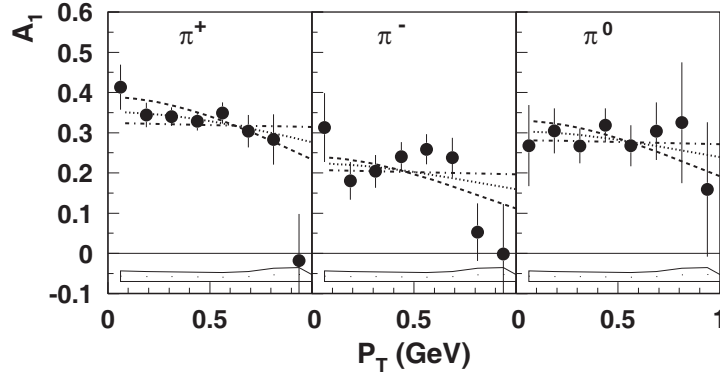

Fig. 14. – The double-spin asymmetry A_1 as a function of transverse momentum of hadrons, P_{hT}, averaged in the $0.4 < z < 0.7$ range. The empty band corresponds to systematic uncertainties. The three curves are calculations for different transverse momentum widths $(0.1, 0.17, 0.25)$ of g_1 at a fixed width for f_1 (0.25) [54].

that the widths of partonic distributions may indeed depend on the spin orientation (see fig. 14). The P_{hT} dependence of the A_1 DSA for positive and negative hadron productions measured recently by COMPASS [79, 80] and HERMES [135] appeared to be well
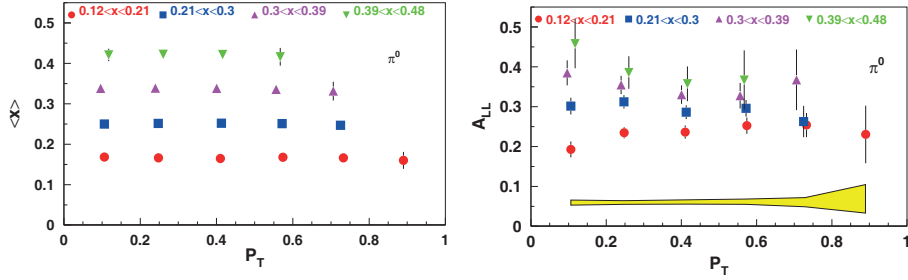
Fig. 15. – The average x versus P_{hT} for $ep \to e'\pi^0 X$ in CLAS kinematics (left), and the double-spin asymmetry in semi-inclusive production of π^0 for different bins in x [83].
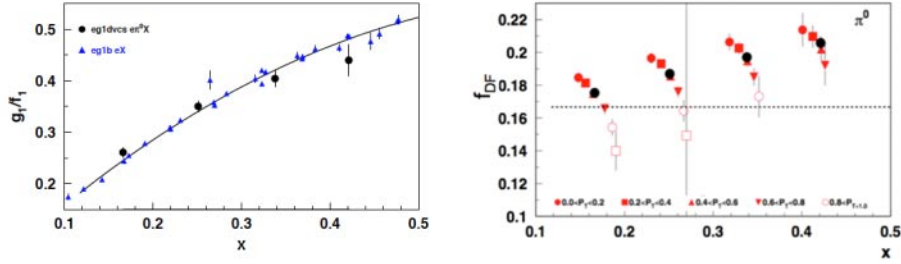

Fig. 16. – The A_1 DSA in semi-inclusive production of π^0, compared to inclusive double-spin asymmetry [83] (left) and dilution factor as a function of x for different bins in P_{hT} (right).

compatible with a constant function. This could indicate that the transverse momentum widths of g_1 and f_1 are the same [54] in the kinematics not dominated by valence quarks. The possible correlation between the x and P_{hT} of the hadron in real experiments is one of the important issues to address in that kind of measurements. Such correlation tends to be much weaker for neutral pions. The new set of measurements with much higher precision for neutral pions performed by the CLAS Collaboration supported the observed complex dependence of the double-spin asymmetry on the transverse momentum (see fig. 15). An important advantage of the π^0 data is the better uniformity and smaller variations of averages of P_{hT} with x due to correlations between longitudinal and transverse momentum of quarks and hadrons. Measurements performed with polarized nuclear targets (NH^3), require a detailed account of the significant nuclear background, and very careful treatment is needed to estimate the dilution factor, which defines the fraction of events originating from polarized quasi-free protons (fig. 16). The double-spin asymmetries in DIS and π^0 SIDIS, in the simple parton model, at large x, where the sea contribution is negligible, are expected to be roughly the same. CLAS measurements of both asymmetries indicate that already at 6 GeV, they are in good agreement (see fig. 16).

Precision measurements using the upgraded CLAS12 detector with polarised NH_3 and ND_3 targets will allow to access the k_T distributions of u and d quarks aligned and anti-aligned with the spin of the nucleon. Projections for the resulting P_{hT} dependence of the double-spin asymmetries for all three pions are shown in fig. 17 for a NH_3 target [42, 44]. Integrated over transverse momentum, the data will also be used to extract the k_T-integrated standard PDFs. Two proposals have been approved to study SSAs with longitudinally polarised target using SoLID detector [40] and Super-Bigbite spectrometer
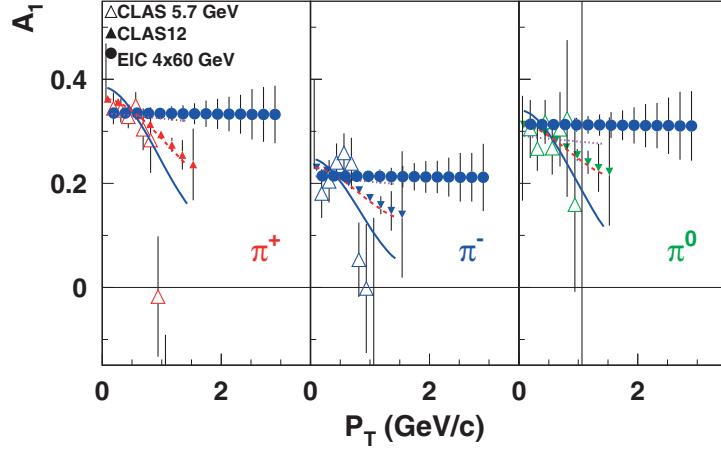
Fig. 17. – Double-spin asymmetry, A_1, for pion production, using the EIC [3] configuration with $4\,\mathrm{GeV}$ electrons and $60\,\mathrm{GeV}$ protons (100 days at $10^{34}\,\mathrm{cm}^{-2}\,\mathrm{sec}^{-1}$), as a function of P_{hT}, compared to published data from CLAS [78] and projected CLAS12 measurements [44].
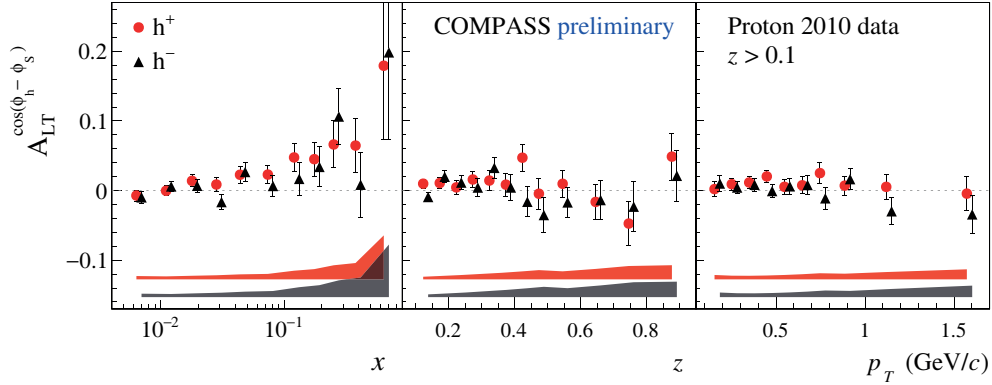

Fig. 18. – The $A_{LT}^{\cos(\phi_h - \phi_S)}$ asymmetry extracted by COMPASS [107, 80]. Colored horizontal bands represent the systematic uncertainties.

with polarised ^{3}He targets. The later one with kaon identification using a RICH detector.

The $A_{LT}^{\cos(\phi_h - \phi_S)}$ DSA provides access to the convolution of the ordinary unpolarized FF with the g_{1T} TMD PDF which parameterizes the distribution of longitudinally polarized quarks in a transversely polarized nucleon

$$(11) \qquad F_{LT}^{\cos(\phi_h - \phi_S)}(x, z, P_{hT}) = \mathcal{C}\left[\frac{\hat{\boldsymbol{h}} \cdot \mathbf{k}_T}{M_N} g_{1T}(x, k_T^2) D_1(z, P_{hT}^2)\right].$$

The g_{1T} twist-2 chiral-even TMD PDF is the imaginary part of the interference terms between S and P wave components. It can be linked (through Lorentz invariance relation) to the twist-3 $g_2(x)$ PDF, which in its turn can be linked to twist-2 helicity PDF $g_1(x)$ using the so-called Wandzura-Wilczek approximation [136]. Measurements of the
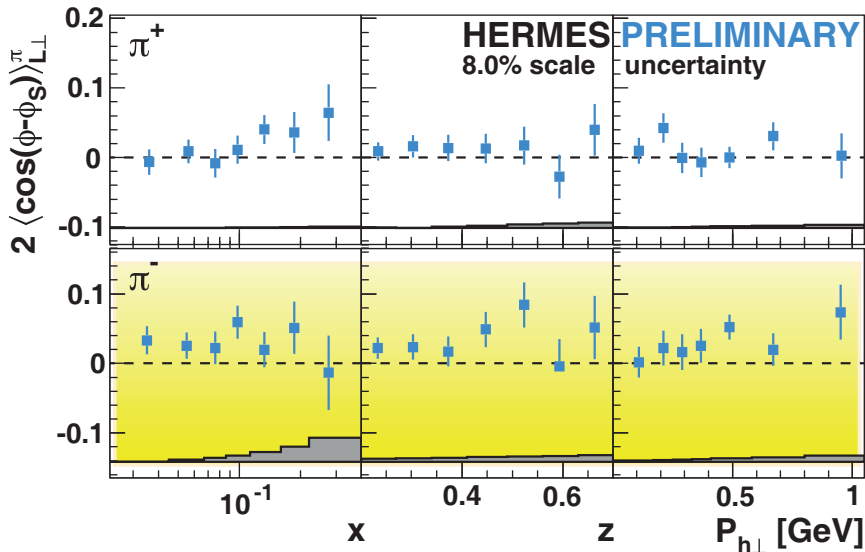
Fig. 19. – The preliminary $A_{LT}^{\cos(\phi_h-\phi_S)}$ asymmetry extracted by HERMES [137]. Horizontal bands represent the systematic uncertainties.

$\cos(\phi_h - \phi_S)$ amplitude by COMPASS and HERMES Collaborations indicate also that the correlation may be significant at large x (see figs. 18 and 19).

In particular at COMPASS, for positive hadrons, the asymmetry is clearly positive increasing up to ≈ 0.1 in the interval of relatively large x ($x > 0.01$). For negative hadrons the effect is less prominent due to larger statistical uncertainties. The observed behaviour and the magnitude of the effect are well in agreement with the available model calculations [136] and with observations made by HERMES. This modulation will be also measured by CLAS12 in the valence region with beam energy 10.6 GeV and transversely polarized HD-Ice target [138].

4. – Higher-twist observables

Twist-3 TMDs, shown in table I, contribute to various observables in SIDIS. They describe quantum-mechanical quark-gluon correlation functions and thus do not have simple partonic interpretation as probability densities. It is interesting to notice that higher-twist asymmetries, especially those not receiving contributions from leading-twist structure functions, were measured and in most of the cases were found not only to be not compatible with zero, but very significant. Good examples are the $\cos\phi_h$ moment of the unpolarized cross-section, $F_{UU}^{\cos\phi_h}$, first measured by the EMC Collaboration, back in the '80s [139, 140], the $\sin\phi_h$ moment depending on the longitudinally target polarization, $F_{UL}^{\sin\phi_h}$, measured by HERMES Collaboration in the '90s [141, 71, 84, 85], and the $\sin\phi_h$ moment depending on the longitudinal polarization of the beam, $F_{LU}^{\sin\phi_h}$, measured at JLab [142-144]. All those measurements were repeated and confirmed later by HERMES, COMPASS and JLab.

The gluon radiation recoil in SIDIS was predicted to lead to observable $\cos\phi_h$ modulations of the SIDIS cross-section, and this effect was proposed by Georgi and Politzer

in the '70s [145] as a clean test of perturbative QCD. The gluon radiation indeed leads to azimuthal dependencies in the semi-inclusive DIS cross-section, but its contribution is significant mainly at large values of P_{hT}.

In 1978, Cahn [25] discussed the origin of $\cos\phi_h$ modulation arising from non-zero intrinsic transverse momenta of partons. Although suppressed by P_{hT}/Q, that modulation (known as the Cahn effect) appeared to be significant and dominating in the $P_{hT} \sim 1\,\text{GeV}$ range. The same mechanism contributes also to the $\cos 2\phi_h$ moments at twist-4 level. Significant azimuthal modulations observed in various experiments indicate the importance of high-twist effects. Additional contribution to $\cos\phi_h$ and $\cos 2\phi_h$ moments could come from processes when the final meson is produced at short distances via hard-gluon exchange, as proposed by Berger in 1980 [26], and may also be significant in the kinematic regime where the ejected meson carries most of the virtual photon momentum. It appeared that the interplay between the parton transverse momentum and spin, the so-called Boer-Mulders effect [18], in addition to leading-twist contribution to the $\cos 2\phi_h$ can also generate subleading contribution to the $\cos\phi_h$ amplitude.

The cross-section modulation $F_{UU}^{\cos\phi_h}$ originates from contributions only at subleading-twist level and is suppressed by M/Q. As far as the structure function $F_{UU}^{\cos\phi}$ is a higher-twist structure function, it can only be accessed at moderate values of Q. Higher-twist observables are a key for understanding long-range quark-gluon dynamics, for instance they can be interpreted in terms of the average transverse forces acting on a quark after it absorbs the virtual photon [146].

In order to simplify the discussion, one can use the so-called Wandzura-Wilczek-type (WW-type) approximation neglecting all quark-gluon-quark correlators. Generically one can decompose higher-twist TMDs into leading-twist terms, current-quark mass terms and the so-called pure interaction-dependent ("tilde") terms. This is accomplished by employing the equations of motion (EOM) and reveals that tilde-terms are not probability densities but quark-gluon correlation functions. Neglecting the tilde- and mass terms is sometimes referred to as the Wandzura-Wilczek approximation [147]. This step can be helpful in phenomenology to disentangle the many contributions to twist-3 SIDIS observables [148-150, 77], and can in certain cases be a numerically useful approximation [81, 151]. Recently the authors of ref. [82] have performed a comprehensive phenomenological study of the cross-section for the production of unpolarized hadrons in SIDIS, computing all twist-2 and twist-3 structure functions within Wandzura-Wilczek-type approximations and compared calculations to the existing experimental data. For the $F_{UU}^{\cos\phi_h}$ structure function one obtains the following result:

$$(12) \qquad F_{UU}^{\cos\phi_h} \simeq \frac{2M}{Q}\, C\left[-\frac{\hat{\boldsymbol{h}}\cdot\mathbf{k}_T}{M_N}xf^\perp D_1 + \frac{\hat{\boldsymbol{h}}\cdot\mathbf{p}_T}{zm_h}xhH_1^\perp\right],$$

where the first term is related to the Cahn effect [25], the second term, strictly speaking is 0 due to the sum rule [11]

$$(13) \qquad\qquad\qquad x\,h^q(x) = 0.$$

Several measurements of $\cos\phi_h$ and $\cos 2\phi_h$ modulations in SIDIS experiments have been published in the past [139, 140, 152, 153]. The CLAS Collaboration measured non-zero cosine modulations for positive pions produced by $6\,\text{GeV}/c$ electrons scattering off the proton [154]. The HERMES experiment has measured cosine modulations of hadrons
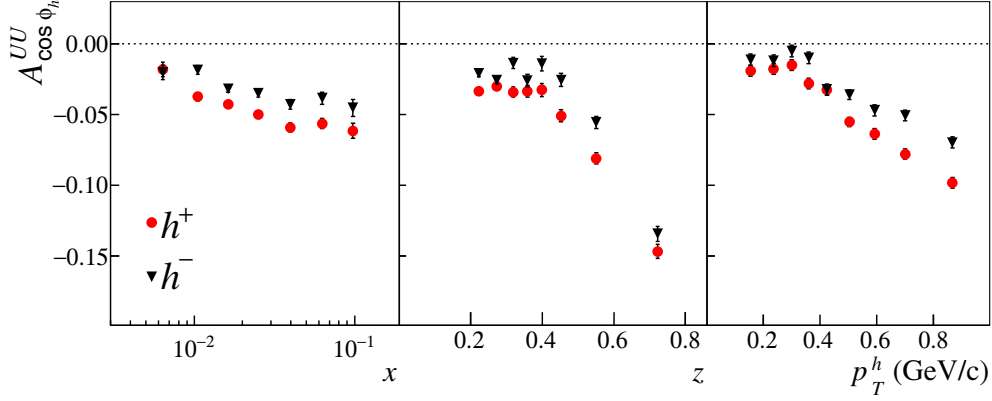
Fig. 20. – The $A_{UU}^{\cos(\phi_h)}$ asymmetry for positive and negative hadron productions as extracted by COMPASS [155].

produced in the scattering of $27.5\,\mathrm{GeV}/c$ electrons and positrons off pure hydrogen and deuterium targets, where the lepton beam scatters directly off neutrons and protons (with only negligible nuclear effects in case of deuterium) [69]. These modulations were determined in a four-dimensional kinematic space for positively and negatively charged pions and kaons separately, as well as for unidentified hadrons. At COMPASS, positive and negative hadrons produced by the $160\,\mathrm{GeV}/c$ muon beam scattering off a ^{6}LiD target have been measured in a three-dimensional grid of the relevant kinematic variables x, z and P_{hT} [155]. In fig. 20 COMPASS results are presented in a one-dimensional representation, $i.e.$ as a function of x, z or P_{hT}, while integrating over the other variables.

The azimuthal modulations have been studied phenomenologically, for instance ref. [156] investigated the effects due to the phase space limitations due to finite beam energies of real experiments as the cosine modulations are very sensitive to the corrections due to limitation of the phase space in experiments. The twist-3 nature of $\cos\phi_h$ modulations could be tested by examining their Q^2 dependence. In fig. 21 the CLAS
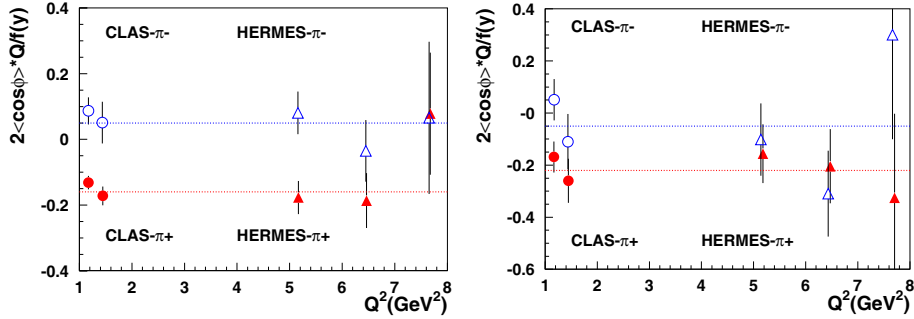

Fig. 21. – The $\cos\phi_h$ modulations in $\pi^\pm$ SIDIS plotted $vs.$ Q^2 for bins with $x \approx 0.19$, and $z \approx 0.35, P_{hT} \approx 0.6\,\mathrm{GeV}$ (left) and $z \approx 0.43, P_{hT} \approx 0.8\,\mathrm{GeV}$ (right). Filled symbols are for π^+ and open symbols for π^-. The triangles CLAS and open symbols are for HERMES [69]. $f(y) = \sqrt{2\epsilon(1+\epsilon)}$.

measurements are compared with the corresponding measurements from the HERMES experiment [69], after taking into account the kinematic factors in the expression of the $\cos\phi_h$ modulation and ϕ_h independent terms. The CLAS and HERMES measurements are found to be consistent with each other in a wide range of Q^2, as shown in fig. 21, indicating that at energies as low as 5–6 GeV, the behaviors of azimuthal modulations are similar to each other. For comparison, the lowest x bin from CLAS and highest x bins from HERMES were used with equal average value of $x \approx 0.19$, $z \approx 0.45$ and $P_{hT} \approx 0.42$ GeV. The CLAS data provides significant improvements in the precision of azimuthal moments for the kinematic region where the two data sets overlap, and they extend the measurements to the large x region not accessible at HERMES, providing an important input for studies of higher-twist effects. The Q^2 dependence of the $\cos\phi_h$ modulation is consistent with the twist-3 nature of the contribution and within statistical uncertainties it is consistent with measurements performed at much higher energies and Q^2. Higher-precision data from 12 GeV upgrade of JLab will provide essential information onto the Q^2 dependence of observables in more details.

Large spin-azimuthal asymmetries observed at JLab for a longitudinally polarised beam [142], which have been interpreted in terms of higher-twist contributions, are also consistent with the corresponding higher-energy measurements at HERMES [157] and COMPASS [155]. Within the same approximation as used in eq. (12), the expressions for the $\sin\phi_h$ modulations in case of polarized beam or target can be written as

$$
(14) \qquad F_{LU}^{\sin\phi_h} \simeq \frac{2M}{Q}\, \mathcal{C}\left[\frac{\hat{\boldsymbol{h}}\cdot\mathbf{k}_T}{M_N}xg^\perp D_1 + \frac{\hat{\boldsymbol{h}}\cdot\mathbf{p}_T}{zm_h}xeH_1^\perp\right],
$$

$$
(15) \qquad F_{UL}^{\sin\phi_h} \simeq \frac{2M}{Q}\, \mathcal{C}\left[\frac{\hat{\boldsymbol{h}}\cdot\mathbf{k}_T}{M_N}xf_L^\perp D_1 + \frac{\hat{\boldsymbol{h}}\cdot\mathbf{p}_T}{zm_h}xh_L H_1^\perp\right].
$$

The distribution e and h_L are twist-3 TMD distribution functions that couple to chiral-odd Collins fragmentation function $H_1^\perp$, contributing to Collins-type terms in $F_{UL}^{\sin\phi_h}$ and $F_{LU}^{\sin\phi_h}$ and can be written in the following way [158, 11]:

$$
(16) \qquad xe = x\tilde{e} + \frac{m}{M}\, f_1,
$$

$$
(17) \qquad xh_L = x\tilde{h}_L + \frac{P_{hT}^2}{M^2}\, h_{1L}^\perp + \frac{m}{M}\, g_{1L}.
$$

The Sivers-type contributions (terms that contain D_1) involve $f_L^\perp$ and $g^\perp$ TMDs, which couple to the leading-twist unpolarized fragmentation function D_1. Some of those functions can be studied in jet production, for instance, the T-odd twist-3 TMD $g^\perp$ gives rise to a $\sin\phi_h$ azimuthal asymmetry in the production of jets [159] in DIS with polarized lepton beams. The higher-twist TMDs attracted a lot of theoretical attention, since the first SSA was observed by HERMES [141]. Some initial model calculations of unpolarized higher-twist TMDs were discussed in refs. [160-164, 129]. A detailed list of recent calculations is presented in ref. [165]. The function $g^\perp$ is an interesting object for theoretical studies. It was shown in ref. [15] that $g^\perp$ has an uncanceled light cone divergence and thus in principle TMD factorization at twist-3 fails. Additional theoretical studies of such functions as $g^\perp$ that arise at twist-3 level are needed to explore twist-3 factorization in detail and determine whether the factorization can be established or not.
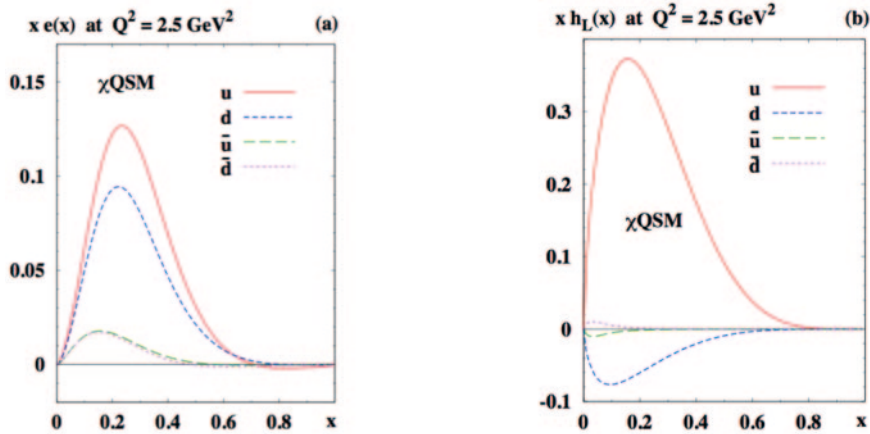
Fig. 22. – The parton distribution functions $xe(x)$ and $xh_L(x)$ from the chiral quark soliton model (χQSM) [172, 175] at $Q^2 = 2.5\,\text{GeV}^2$.

4`1. *Model calculations*. – An important question that one could ask is whether twist-3 functions that we discuss are different from zero or not. Model calculations can certainly shed light on this matter. In fact many model calculations indicate sizable twist-3 functions, see for example ref. [166] where twist-3 fragmentation functions were studied.

The WW approximation that we discussed in the previous subsection is certainly useful for numerical estimates but it removes the richness of the largely unexplored but attractive non-perturbative physics of quark-gluon correlations. This richness is precisely the important motivation to study subleading-twist effects [167, 14].

Higher-twist TMDs and parton distribution functions of quarks are expressed in terms of hadronic matrix elements of bilinear quark-field correlators which can be studied in quark models [160]. Quark models have been shown to give a useful description of leading-twist TMDs and related SIDIS observables, provided one applies them carefully within their range of applicability.

Quark models with interactions allow one to model also the interaction-dependent tilde-terms. There are several model calculations of the twist-3 PDFs e and h_L: MIT bag model [160, 161, 129], diquark spectator model [162], instanton QCD vacuum calculus [168, 169], chiral quark soliton model [170, 163, 164, 171, 172], and the perturbative light-cone Hamiltonian approach with a quark target [173, 174]. In these calculations there are no contributions from either strange or sea quarks, except for the chiral quark soliton model. Figure 22 shows the parton distribution functions $e(x)$ and $h_L(x)$ calculated in the chiral quark soliton model [172, 175] at $Q^2 = 2.5\,\text{GeV}^2$. The bag model has given several powerful results and predictions of PDFs as well as TMDs. It is a relativistic model where quarks and antiquarks are excitations inside the confined bag. It is generally assumed that the proton wave function is invariant under the $SU(6)$ spin-flavor symmetry. In the case of two-body problems, this symmetry leads to a proportionality between the different flavor components. The contribution to $e(x)$ in the bag is entirely due to the bag boundary, and therefore to the quark-gluon-quark correlation. The result of the model calculation of the twist-3 $e^u(x)$, $h_L^u(x)$, as well as of the unpolarized distribution $f_1^u(x)$, is shown in fig. 23. On the other hand, the function $h_L(x)$ contains twist-2 and pure twist-3 contributions.
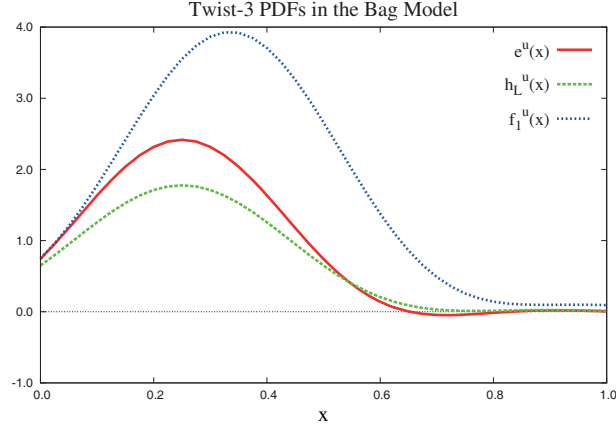
Fig. 23. – The functions $e^u(x)$, $h_L^u(x)$, and $f_1^u(x)$ calculated in the bag model [160].

Although it is a popular assumption that pure twist-3 (and mass) terms are small [176, 10, 81, 177], this has rarely been justified by theoretical calculations. Indeed, recent calculations using light-front wave functions (LFWFs) [178], taking into account the contribution from both the three valence quark (qqq) and three-quark plus one gluon ($qqqg$) Fock state of the nucleon, indicate that the pure twist-3 contributions can be very significant in certain kinematics. The LFWFs are modeled using a parametrization derived from the proton distribution amplitudes, with parameters fitted to the available phenomenological information on the unpolarized leading-twist quark and gluon collinear parton distributions. Figure 24 presents the light-front model results for the twist-2 contribution ($m/M f_1$), the pure twist-3 terms ($\tilde{e}$) and the total results, for both the up and down quark.

The twist-3 distributions have been recently also studied in lattice QCD calculations. The ratio of Fourier transformed to conjugate quark separation b_T-space twist-3 TMD e, integrated over momentum fraction x and over the unpolarized TMD f_1, likewise integrated and Fourier-transformed is shown in fig. 25. The framework for these calculations
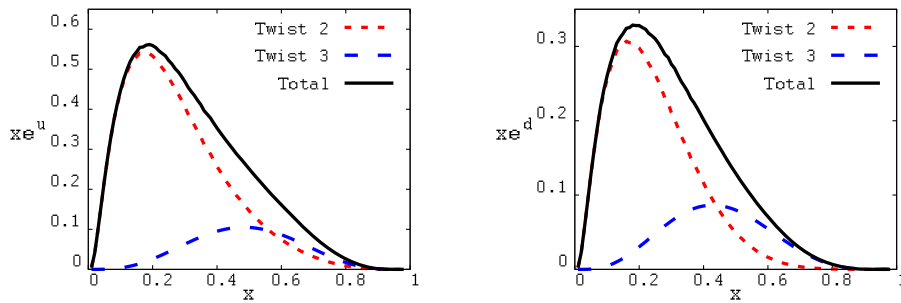

Fig. 24. – Results for the PDF $xe(x)$ as a function x for the up (left panel) and down (right panel) quark [178]. Red short-dashed curve: twist-2 contribution ($m/M f_1$); blue long-dashed curve: pure twist-3 contribution ($\tilde{e}$); solid curve: total results, sum of the twist-2 and twist-3 contribution.
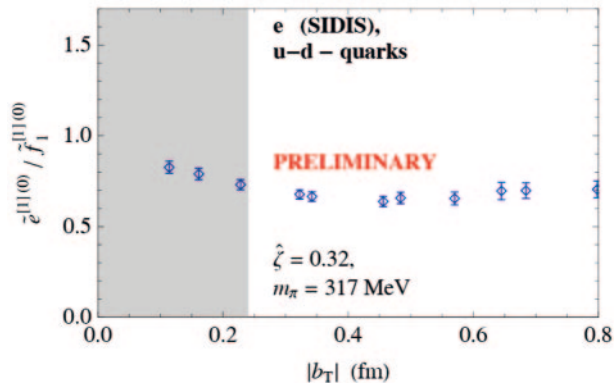
Fig. 25. – The ratio of isovector $u - d$ combination of quark flavors for e and f_1 [181]. The shaded area represents the region in which discretization effects may be significant.

is described comprehensively in refs. [179, 180]. Data were obtained from a lattice QCD calculation of the proton matrix elements defining these TMDs, where the staple-shaped gauge link in the relevant quark bilocal operator extends in the direction appropriate for the SIDIS process. The Collins-Soper-type parameter $\hat{\zeta} = v \cdot P/(|v||P|)$ characterizes the rapidity difference between the proton momentum P and the direction of the staple legs v. The phenomenologically most relevant range of $\hat{\zeta}$ lies appreciably above the value accessed in this calculation, which was moreover performed at an artificially high pion mass. While lattice QCD calculations closer to the physical case remain to be performed, extraction on lattice is consistent in sign and magnitude with simple model calculations discussed above and presented in fig. 23. One can see that lattice computations suggest that e has almost the same relative size as twist-2 f_1.

With several functions contributing to the same observable one faces a difficult task when dealing with subleading twist in SIDIS, but it is important to stress that each of them provides a different and independent view of the quark-gluon dynamics in the nucleon or in the fragmentation process. The importance of these observables for spin physics and QCD is very high, indeed these were the first instances that single spin phenomena in SIDIS have been measured and this has triggered important theoretical developments. Both structure functions, $F_{LU}^{\sin \phi_h}$ and $F_{UL}^{\sin \phi_h}$, were subject to numerous theoretical and phenomenological studies [182-185, 149, 186, 170, 150, 187-190, 77, 191-195], see also [196, 197, 159, 198, 11]. Nevertheless there is presently no satisfactory understanding on which are the functions of origin of these modulations from the point of view of a quantifying contribution of the underlying functions.

Other subleading structure functions have also been studied [199-201] though less extensively, since there is far less data available, though measurements of some subleading functions were reported [202, 137, 80]. The TMDs e and $g^\perp$ are pure twist-3 interaction-dependent quark-gluon correlators, *i.e.* $e = \tilde{e}$ and $g^\perp = \tilde{g}^\perp$ up to current quark mass terms, and hence vanish in the Wandzura-Wilczek-type approximation discussed above. This means that in this approximation the entire $F_{LU}^{\sin \phi_h}$ would vanish, while in experiment a clearly non-zero effect is seen [142, 203].

A detailed study of non-perturbative properties of subleading twist TMDs has been performed recently by Lorce and collaborators [165]. The formalism to describe unpolarized higher-twist TMDs in the light-front framework based on a Fock-space expansion
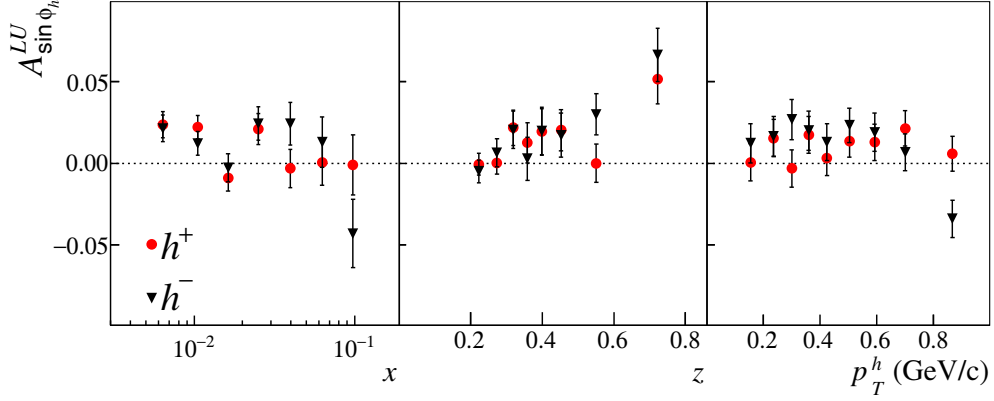
Fig. 26. – The $A_{LU}^{\sin(\phi_h)}$ asymmetry extracted for positive and negative hadron productions by COMPASS [155].

of the nucleon state in terms of free on-shell parton states has been developed, and some numerical results in a practical realization of this picture performed by the light-front constituent quark model. The results from the light-front constituent quark model were also compared to available phenomenological information, showing a satisfactory agreement.

In figs. 26 and 27 COMPASS (deuteron) and recent HERMES (deuteron, proton) results for $A_{LU}^{\sin(\phi_h)}$ asymmetries are shown as a function of x, z and P_{hT}.

Since the structure functions F_{LU} and F_{UL} contain kinematical terms depending on the beam energy for given kinematics, as well as additional $1/Q$ suppression factor, direct comparison of ratios of structure functions involved in those observables among different experiments requires accounting for those terms. After corrections the data seem to be consistent also between CLAS and HERMES $A_{LU}^{\sin \phi_h}$, see fig. 28. Recent
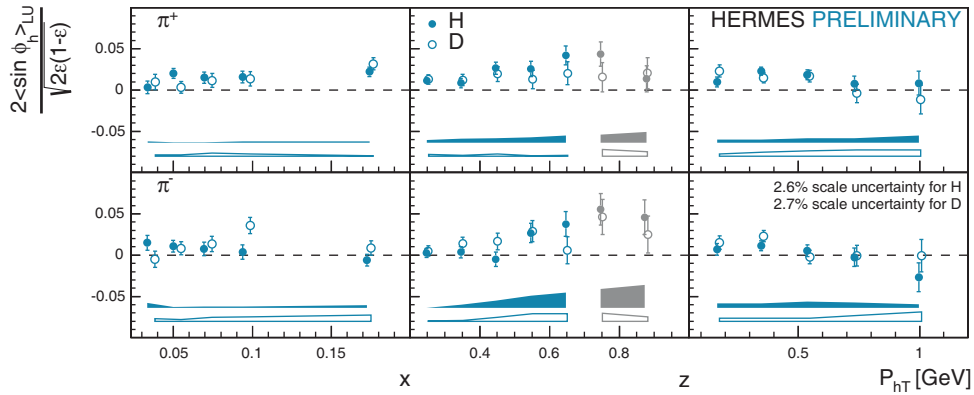

Fig. 27. – The preliminary $A_{LU}^{\sin(\phi_h)}$ amplitudes for charged pions extracted from data on unpolarized hydrogen (H) and deuterium (D) targets by HERMES [204]. The asymmetries are corrected for the depolarization factor.
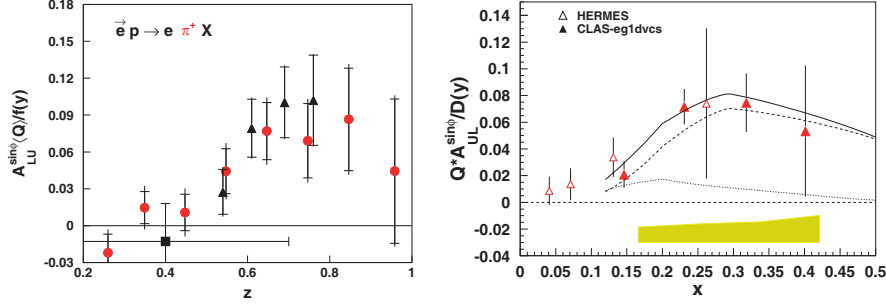
Fig. 28. – The comparison of SSA $A_{LU}^{\sin\phi}$ as a function of x for neutral pions at HERMES [203] and CLAS for similar average P_{hT} [143] (left panel). Both Asymmetry moments are multiplied by the kinematic factor $Q/f(y)$. The right panel shows the comparison of SSA $A_{UL}^{\sin\phi}$ for neutral pions at HERMES and CLAS [83] (right). The factor $D(y)$ for longitudinally polarized case is given in eq. (1). The dashed and dotted lines are twist-3 calculations from from Sivers and Collins type terms [205, 206], respectively.

high-precision measurements of $A_{UL}^{\sin\phi_h}$ performed at COMPASS are also consistent with similar measurements at HERMES, see fig. 29. Both asymmetries exhibit a similar kinematical behaviour and, more importantly a similar flavor dependence. Accounting for the difference in energies and average y in all comparisons was done by dividing by the kinematic factors defined in eq. (1) (for $A_{UL}^{\sin\phi_h}$ the $D(y) = \sqrt{2\epsilon(1+\epsilon)}$). Comparison of $A_{LU}^{\sin\phi_h}$ and $A_{UL}^{\sin\phi_h}$ for π^+ and π^0 (see fig. 30) indicates, that in both cases they are consistent with each other. Latest measurements of $A_{UL}^{\sin\phi_h}$ by CLAS [83] for all pion flavors is consistent with HERMES measurements, confirming that π^+ and π^0 show similar behaviour for both $A_{LU}^{\sin\phi_h}$ and $A_{UL}^{\sin\phi_h}$.

Understanding of quark-gluon dynamics is crucial for interpretation of upcoming SIDIS data from Jefferson Lab 12 GeV upgrade, where studies of TMDs are one of the main driving forces. Significantly higher, compared to JLab12, P_{hT} range accessible at EIC would allow studies of transverse momentum dependence of various distribution and
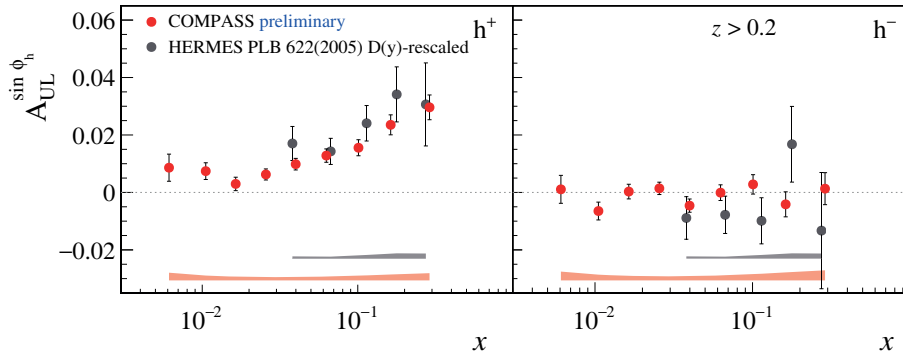

Fig. 29. – The preliminary results for $A_{UL}^{\sin(\phi_h)}$ obtained by COMPASS [79,80] are shown together with the HERMES results [157]. Presented results are not rescaled for $1/Q$. HERMES results are rescaled for $D(y)$.
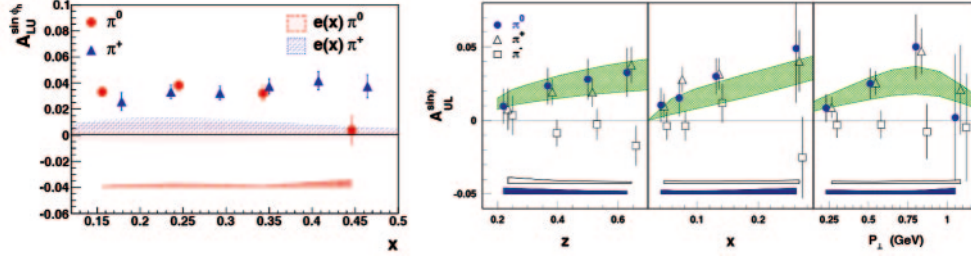
Fig. 30. – Left panel: comparison of $A_{LU}^{\sin(\phi_h)}$ for π^+ and π^0 from CLAS data [143] for the same average $P_{hT} = 0.38$ GeV and $0.4 < z < 0.7$. The error bars correspond to statistical and bands to systematic uncertainties. The hatched band shows model calculations involving only the Collins effect for π^0. Right panel: $A_{UL}^{\sin(\phi_h)}$ for different flavors using HERMES data [84]. Error bars include statistical uncertainties only. Filled and open bands at the bottom of the panels represent the systematic uncertainties for neutral and charged pions, respectively. The shaded areas show a range of predictions of a model calculation [207, 148] applied to the case of π^0 electroproduction.

fragmentation functions as well as transition from the TMD regime ($P_{hT}/z \ll Q$) to the collinear perturbative regime ($P_{hT}/z \sim Q$). Measurements of spin and azimuthal asymmetries as a function of the final hadron transverse momentum at EIC will extend (see fig. 31) measurements at JLab12 [208] to significantly higher P_{hT} and lower x and will provide access to studies of TMDs beyond the valence region. A much higher Q^2 range accessible at EIC would allow for studies of the Q^2 dependence of different higher-twist spin-azimuthal asymmetries (fig. 31), which, apart from providing important information on quark-gluon correlations, are needed for understanding possible corrections from higher-twists to leading-twist observables.

Both Jefferson Lab12 and future EIC will measure also other azimuthal moments arising due to different quark-gluon-quark interactions. Many of them have been already measured by HERMES and COMPASS in the corresponding kinematical regions, including $A_{LL}^{\cos\phi}$ and $A_{UT}^{\sin\phi_S}$, see figs. 33, 34 and 35. A common feature of all higher-twist asymmetries is the increase at large x.
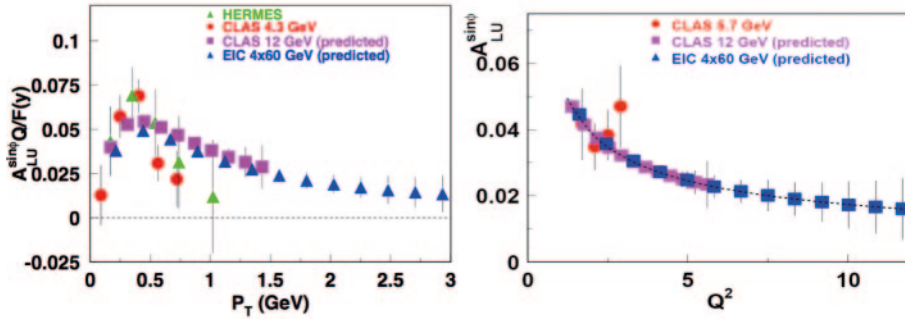

Fig. 31. – Projections for higher-twist lepton spin asymmetry $A_{LU}^{\sin\phi}$ for positive pion production, using 4 GeV electrons and 60 GeV protons (100 days at 10^{34} cm^{-2} sec^{-1}), as a function of P_{hT} (left) and Q^2 (right) compared to published data from CLAS [142] and HERMES [203] and projected CLAS12 [208] in one x, z bin ($0.2 < x < 0.3$, $0.5 < z < 0.55$).
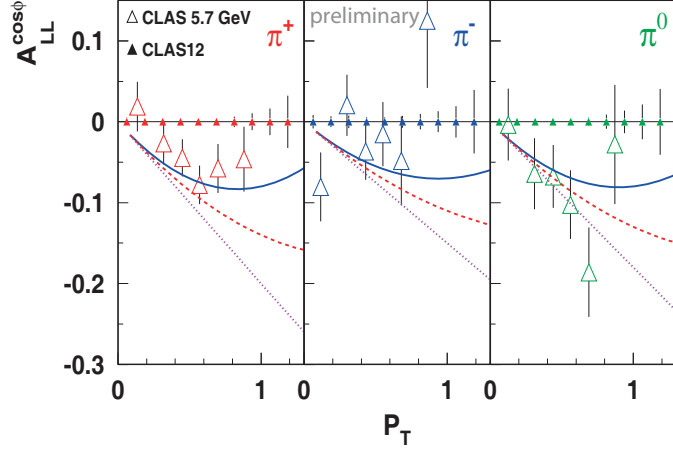
Fig. 32. – The $A_{LL}^{\cos(\phi_h)}$ as a function of the hadron transverse momentum. The filled triangles show projected uncertainties from approved JLab12 measurements [42] compared to 5.7 GeV preliminary result (open triangles). The lines correspond to model calculations from ref. [54].

The $F_{LL}^{\cos \phi_h}$ structure function can be presented as follows:

$$(18) \qquad F_{LL}^{\cos \phi_h} \simeq \frac{2M}{Q} \mathcal{C} \left[-\frac{\hat{\boldsymbol{h}} \cdot \mathbf{k}_T}{M_N} x g_L^\perp D_1 - \frac{\hat{\boldsymbol{h}} \cdot \mathbf{p}_T}{z m_h} x e_L H_1^\perp \right].$$

Within the WW-type approximation the e_L vanishes and we remain with $x g_L^\perp \simeq g_{1L}$ PDF. The corresponding double-spin asymmetry is an analogue of the aforementioned Cahn effect, but for the polarized (helicity) cross-section [54]. In figs. 32 and 33 JLab and COMPASS results for this DSA are shown.

The $A_{UT}^{\sin \phi_S}$ subleading-twist SSA is a peculiar term, since within the WW-type approximation it can be interpreted as a combination of Sivers and Collins constituents
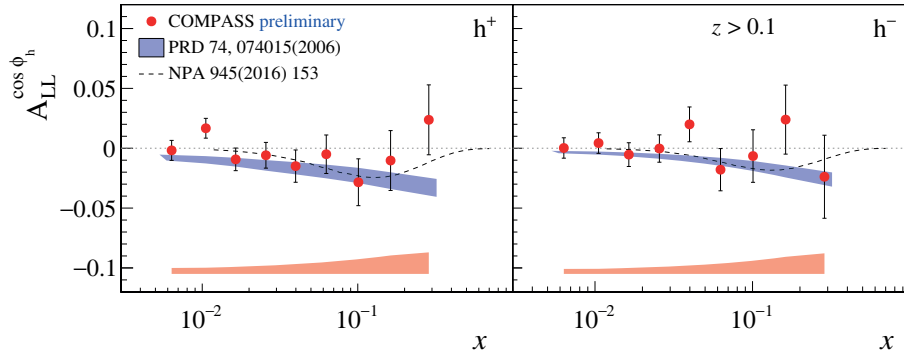

Fig. 33. – The preliminary results for $A_{LL}^{\cos(\phi_h)}$ obtained by COMPASS [79,80] are shown together with available model predictions [54, 209].
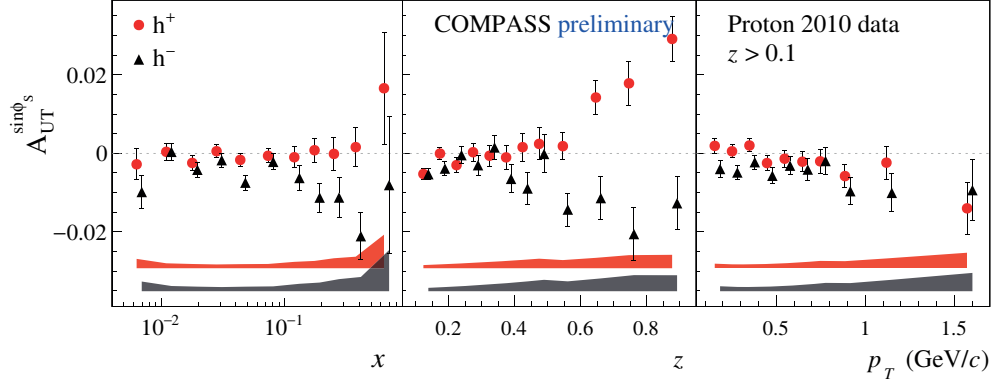
Fig. 34. – The $A_{UT}^{\sin(\phi_S)}$ asymmetry extracted by COMPASS [107, 80].
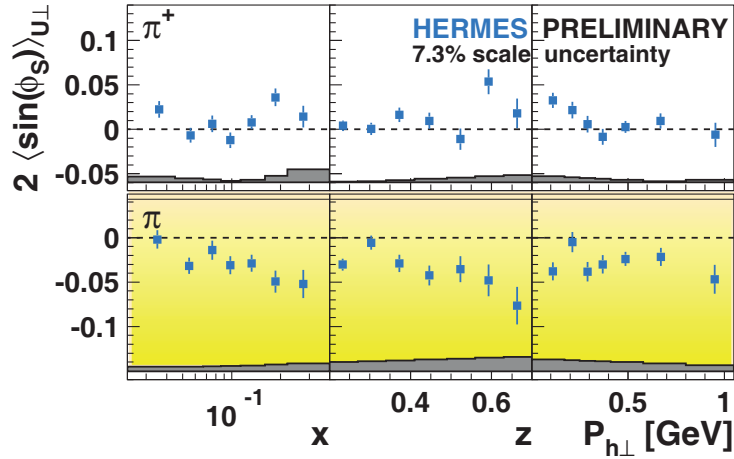
Fig. 35. – The preliminary $A_{UT}^{\sin(\phi_S)}$ asymmetry extracted by HERMES [137].

(within WW-type approximation). The corresponding structure function reads:

$$
(19) \qquad F_{UT}^{\sin \phi_S} \simeq \frac{2M}{Q} \, \mathcal{C} \left\{ x f_T D_1 + \frac{\mathbf{k}_T \cdot \mathbf{p}_T}{2 M_N z m_h} \left[x h_T - x h_T^{\perp} \right] H_1^{\perp} \right\}.
$$

If one employs the WW-type approximation, then $x f_T \simeq f_{1T}^{\perp}$ is a Sivers type and $x h_T - x h_T^{\perp} \simeq -2 h_1$ is a Collins-type contribution. COMPASS and HERMES results for this SSA are presented in figs. 34 and 35. In both cases the asymmetry exhibits a non-zero signal at large z, in particular, for negative hadrons.

5. – Flavor dependence of spin-azimuthal asymmetries

One of the important challenges in phenomenological fits is to disentangle the flavor dependence of the TMD PDFs from the measurements for a limited set of final particle

types. The difficulty is that in the corresponding cross-section the TMD PDFs are convoluted with the fragmentation functions to the specific hadrons and these are summed over the flavor of the parton. Thus having SSA measurements for as large a number of final hadron types as possible would allow removing some of the assumptions about the flavor dependence of the corresponding TMDs, Sivers PDFs, in particular. Measurements with different final state hadrons are crucial for the understanding of the dynamics and sorting out contributions due to spin-orbit correlations occurring in the initial distributions and in final stage of hadronization.

For example, electroproduction of neutral pions has several important advantages: 1) suppression of higher-twist contributions at large hadron energy fraction z [210], which are particularly important at JLab energies where small z events are contaminated by target fragmentation; 2) the absence of ρ^0 production which complicates the interpretation of the charged single-pion data; 3) the fragmentation functions for u and d quarks to π^0 are the same in first approximation; and 4) suppression of spin-dependent fragmentation for π^0's, due to the roughly equal magnitude and opposite sign of the Collins fragmentation functions for up and down quarks [86, 97, 211-213]. In addition it was shown that the longitudinal photon contribution is suppressed in exclusive neutral pions production [214] with respect to the transverse photon contribution, which is higher twist, suggesting that longitudinal photon contribution to SIDIS π^0 will also be suppressed. At large x, where the sea contribution is negligible, π^0 multiplicities and double-spin asymmetries will provide direct info on the fragmentation function of u and d quarks to π^0. These factors simplify the interpretation of π^0 observables, such as single- and double-spin asymmetries. Furthermore, neutral pions are straightforward to identify with little background using the invariant mass of two detected photons. Similar, important features, like equal fragmentation functions for u and d exhibit also the production of charged pion pairs.

6. – Dihadron production

Measurements of Collins asymmetries, $A_{UT}^{\sin(\phi_h+\phi_S)}$, at HERMES and COMPASS, confirm non-zero Collins fragmentation functions, which are likely generated due to correlation of the transverse spin of fragmenting quarks and the orbital motion of $q\bar{q}$ pairs [215]. That means that the leftover pair of the $q\bar{q}$ will end up in the second hadron. Hadron pair production allows the possibility of the extraction of the transversity distribution in a complementary way to the single-hadron production case and was used in the extraction of transversity in an analysis with combined electron-proton and proton-proton data [216]. In order to extract the transversity distribution from single-hadron production, the Collins function should be determined through the measurement of azimuthal asymmetries in the distribution of two almost back-to-back hadrons in e^+e^- annihilation [217]. The Belle and BaBar Collaborations measured this asymmetry [211, 92, 218], making the first ever extraction of h_1^q possible from a simultaneous analysis of $ep^\uparrow \to e'\pi X$ and $e^+e^- \to \pi\pi X$ data [93].

In spite of this breakthrough, some issues still hinder the extraction of transversity from single-particle-inclusive measurements. The most crucial issue is the treatment of evolution effects, since the measurements were performed at very different energies. The convolution $h_1^q \otimes H_1^{\perp\,q}$ involves the transverse momentum of quarks. Hence, its evolution should be described in the framework of the transverse-momentum-dependent factorization [219, 49]. Quantitative explorations in this direction suggest that neglecting evolution effects could lead to overestimating transversity [220]. The so-called TMD
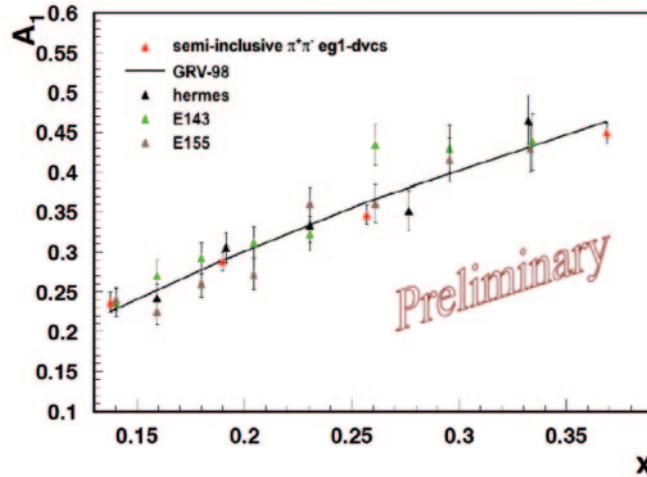
Fig. 36. – The double-spin asymmetry in semi-inclusive production of $\pi^{\pm}$ pairs, compared to inclusive DIS measurements from HERMES [228], CLAS [229] and SLAC E143 [230] and E155 [231] experiments.

framework has been extensively studied [110] (*e.g.* Bessel weighting treatment of cross-sections [221]). The first extraction of transversity with TMD evolution was presented in refs. [222, 223] and was found to be compatible with earlier studies without full account of TMD evolution from refs. [93, 224] thus confirming an idea that in ratios evolution effects generically cancel to a certain extent.

In this context, it is of paramount importance to extract transversity in an independent way, requiring only standard collinear factorization where the above complications are absent (see, *e.g.*, refs. [225, 226] and references therein). Results of the newest analysis from ref. [216] are compatible with refs. [222, 223, 93, 224] and with extraction of transversity that takes into account lattice QCD calculations of tensor charge done in ref. [227], even though some tension still remains among various results.

The semi-inclusive deep inelastic production of two charged pions with small invariant mass,

$$\ell(l) + N(P) \rightarrow \ell(l') + H_1(P_1) + H_2(P_2) + X,$$

which was suggested as a complementary source of information on the quark-gluon dynamics, bears similar features. The double-spin asymmetry of pion pair production has been measured at JLab and shown to be consistent with inclusive DIS asymmetry. Although dihadron production in SIDIS requires higher energies and Q^2 than single-hadron SIDIS, measurements of double-spin asymmetries at CLAS (see fig. 36) are already at $5.7\,\text{GeV}$ compatible with simple leading-twist predictions for the equality of double-spin asymmetries in eX, $e\pi^+\pi^- X$, and $e\pi^0 X$, assuming that the sea quark contributions are negligible at large x and fragmentation functions sum of charged pions are flavor independent.

CLAS measurement of the double-spin asymmetry from inclusive DIS (also from HERMES and SLAC) are consistent with CLAS measurements of double-spin asymmetry in charged pion pair production. At low energies the multiplicities are low and one has to
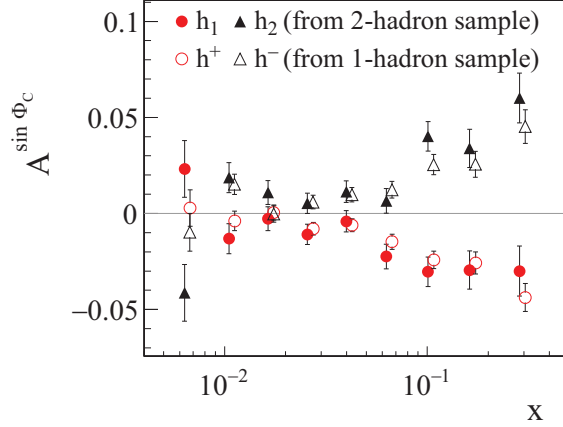
Fig. 37. – Comparison of the Collins asymmetries for single (full red circles) and di-hadrons (full black triangles) from COMPASS measured as function of x [232].

apply cuts on the missing mass of the final state to avoid contributions from exclusive states.

Studies of integrated values of Collins asymmetries in the single-hadron sample were shown to be the same as the Collins-like asymmetries of di-hadron sample which in turn are related with the integrated values of di-hadron asymmetry (see fig. 37), suggesting that both the single-hadron and di-hadron transverse-spin-dependent fragmentation functions are driven by the same underlying mechanism [232].

Two experiments have been approved at JLab to study dihadrons with transversely polarized targets. Combination of hydrogen measurements with CLAS12 [233] and ^{3}He with SoLID [234] (see fig. 38) would allow to perform a complementary to the TMD method flavor decomposition of the transversity distribution.

The interpretation of di-hadron production, as well as the interpretation of single-hadron production is intimately related to contributions to those samples from vector mesons. The general procedure for SIDIS analysis, so far, required estimates of the contribution of diffractive ρ^0, so theoretical studies can account for their contribution. Since the spin-dependent fragmentation (Collins function) of ρ mesons is very different from
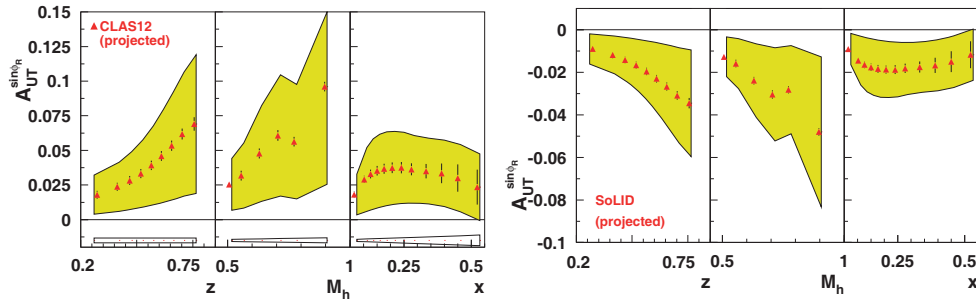

Fig. 38. – The transverse spin-dependent azimuthal asymmetry, $A_{UT}^{\sin \phi_R}$ predicted in approved measurements by CLAS12 on proton [233] (left) and SoLID on neutron [234] (right).
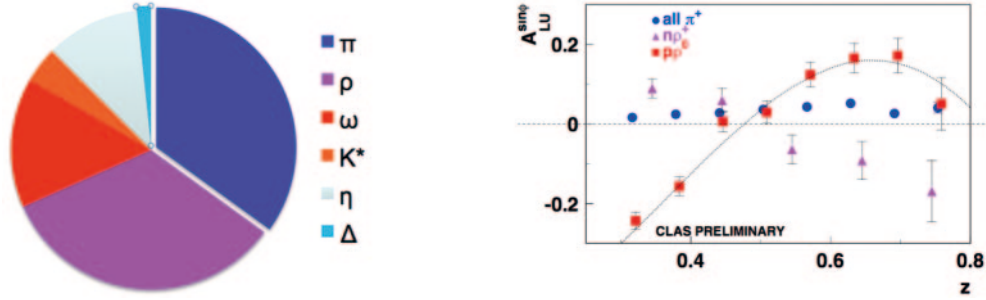
Fig. 39. – Left panel: the fraction of pions in $ep \to e'\pi X$ in HERMES kinematics (27.5 GeV), produced directly from the string in PYTHIA MC (shown as π) and from different decay channels (ρ, ω, K^*, η and Δ). Right panel: $A_{LU}^{\sin\phi}$ asymmetry measured by CLAS on hydrogen target, for final state π^+ originating from exclusive $\pi^+\pi^-$ events dominated by ρ^0 (red squares), from exclusive $\pi^+\pi^0$ events dominated by ρ^+ (magenta triangles) and integrated over all sources (blue circles) [236].

pions, in fact is predicted to have an opposite sign [235], the final interpretation of pion asymmetries will be very sensitive to the relative fraction of pions coming from vector meson decays. The fraction of pions coming from correlated di-hadrons in general, and the ρ decays, in particular, produced in the region of $P_{hT}/z < Q$, contribute to the region $P_{hT}/z > Q$, due to much smaller z of decay pions, making the interpretation of data more complicated. The PYTHIA based MC suggests that the dominating fraction of pions is indeed coming from vector meson decays (see fig. 39). Measurements of SSA performed by CLAS indicate that there is a significant asymmetry in single-pion sample originating from ρ's, which is also very different for different vector mesons. The size of the asymmetry reaches $\sim 20\%$ and is opposite for π^+ originating from exclusive ρ^+ and ρ^0 decays [236].

Significant single-beam spin asymmetries were predicted in di-hadron production for several angular correlations. The usual $\sin(\phi_R)$ single-beam spin asymmetry [237] involves subleading-twist functions in the so-called "collinear kinemaitcs" that involves the measurement of only the relative transverse momenta of the hadron pair. Recently, a new leading-twist single-beam spin asymmetry involving the helicity-dependent DiFF $G_1^\perp$ has been proposed [238], in analogy with the target single spin asymmetry in ref. [239], which requires the measurement of both total and relative transverse momenta of the pair. Yet another leading-twist beam spin asymmetry involves the so-called fracture functions [240], where one of the hadrons is produced in the current region by the fragmenting parton, while the second one is produced in the target region by the target remnant. CLAS preliminary measurements [241] indicated a very significant non-zero beam-spin asymmetry A_{LU} both on ^{2}H and NH$_3$ targets. Non-zero single-spin asymmetries (A_{LU}) have also been observed in back-to-back pion and proton electroproduction [242], indicating that spin-orbit correlations between hadrons may be very significant. While this opens a new avenue for studies of the complex nucleon structure in terms of quark and gluon degrees of freedom, it also suggests that there are likely no uncorrelated hadrons in SIDIS.

7. – Precision measurements of TMDs

The main mission of the experimental exploration of 3D momentum and spatial structure of the nucleon by Jefferson Lab and other facilities in the world is providing the scientific community with unbiased data on observables that can be uniquely interpreted
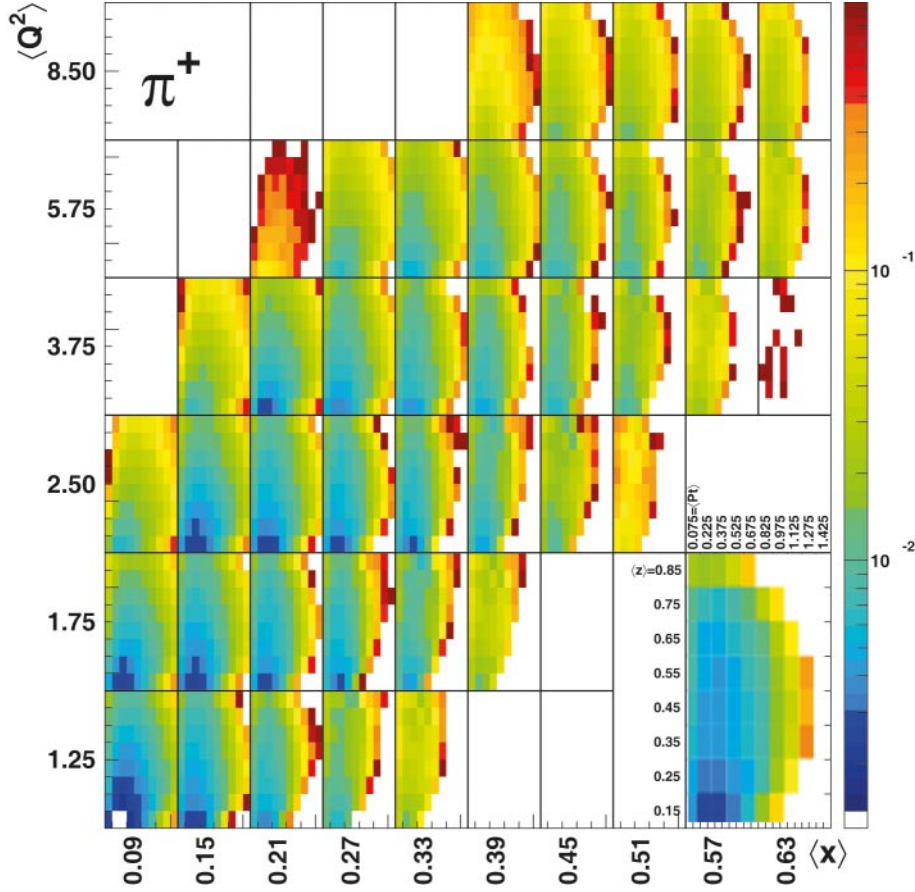
Fig. 40. – The CLAS12 4D kinematical acceptance. The small insert shows an example of 2D bin in z vs. P_{hT} in each of 2D bins in x and Q^2.

in theoretical and phenomenological models, *i.e.* cross-sections, multiplicities, asymmetries, structure functions. It is paramount that experimental results are not influenced by theoretical and/or phenomenological expectations and in this sense a blind analysis will be the most desirable one. Of course in order to achieve such a degree of unbiased measurements one will need to carefully study all pitfalls and limitations of data analysis itself. Experimental Halls of Jefferson Lab are likely to work together on issues related to interpretation and extraction of experimental data.

Although the interest in TMDs has grown enormously, we are still in need of a consistent theoretical and phenomenological description spanning the full kinematic regime covered by the (un)polarized world-data. Some TMDs have been already phenomenologically extracted, mainly from analyzing azimuthal distributions of single hadrons in SIDIS. To obtain a full picture about the 3D momentum structure of the partons in the nucleon from high to low x, it is important to connect the theoretical approaches to extract TMDs including evolution. The studies of 3D PDFs in general, and TMDs in particular, require a lot more attention to uncertainties due to input parametrizations, than in 1D case, as more degrees of freedom and bigger number of input parameters

may generate biased model uncertainties. For example it was argued, based on studies using the mPYTHIA MC generator, that the current extractions of the Sivers PDF might be significantly underestimated [119]. Thus, improvements in estimating the true relative size of the Sivers term in the cross-section would be needed in future precision studies.

The 3D partonic structure accessible in hard scatterings is rich and complex. The understanding of the contributions to the final transverse-momentum dependence of different azimuthal moments in the cross-section will require detailed studies. Monte Carlo event generators accounting for spin-orbit correlations will be crucial to study the dependence on different model inputs, as well as sensitivity of the extraction of underlying TMDs on various experimental uncertainties including acceptances, resolutions and radiative corrections. The acceptances of wide angle detectors are already themselves pretty complicated (see fig. 40).

All that makes the development of a framework for testing different extraction procedures a high priority task for the community involved in studies of 3D PDFs. Development of realistic Monte Carlo generators accounting for TMD evolution effects, spin-orbit and quark-gluon correlations will be a great support for a multifaceted effort to study the fundamental 3D structure of matter.

The future 3D nucleon structure extraction framework should include in addition to extraction procedures a library of 3D PDFs [243-245] and MC simulation frameworks using that library as input and allowing to check the quality of extracted PDFs for specific experimental conditions in a full range of accessible kinematics.

7 1. *Radiative moments in unpolarized SIDIS*. – The corrections due to radiative effects in SIDIS are on the interface of the theory and experiment, and require joint focused activities on both the theoretical and experimental parts. While the theory effort addresses theoretical uncertainties of Radiative Corrections (RC) constrained by a lack of knowledge of the hadronic structure, the experimental approach is on the methodology of data analysis. Currently there are no exact calculations of RC to SIDIS for arbitrary polarizations, with all available calculations representing various kinds of approximations. Model-independent RC can be and must be accounted for exactly in modern measurements in SIDIS within a new procedure of RC of experimental data using sets of semi-inclusive and exclusive Structure Functions (SFs). A self-consistent approach is currently available only for the unpolarized target. Possible (reasonable) approximations used in the literature and data analysis practice include: i) soft photon approximation, ii) leading log approximation, iii) peaking approximation, iv) Compton-peak approximation, and v) using different Monte Carlo generators (*e.g.*, Radgen). The soft photon approximation is very convenient because RC is factorized at the Born cross-section and completely cancels in spin asymmetries, but is wrong because of hard photon emission that can not be neglected even in experiments with a much poorer accuracy comparing to the SIDIS experiments in JLab. The leading log (and peaking) approximation could estimate RC from hard photon with a semi-inclusive process but is not applicable for exclusive radiative tail. The Compton-peak approximation was good for the elastic radiative tail in DIS, but estimates show that it will not work even for the exclusive radiative tail. The most popular Monte Carlo-based approximation uses the generator Radgen [29] for generating radiative photons and evaluating RC based on simulated samples (*e.g.*, with and without using Radgen). Unfortunately this approach is not applicable for analysis of azimuthal asymmetries in SIDIS, because key parts of the cross-section responsible
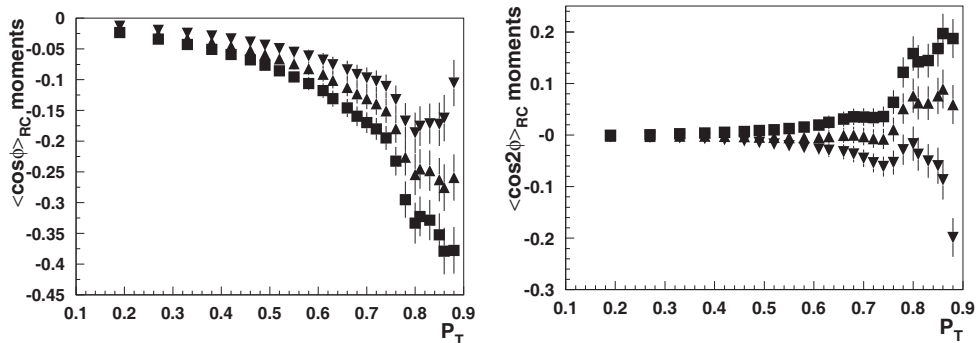
Fig. 41. – Left panel: sensitivity of the $\cos\phi$ moment generated by radiative effects to the ϕ dependence of three different structure functions with $\cos\phi$ input amplitudes equal to -5% (squares) -10% (triangles up) and -15% (triangles down) calculated from haprad2.0 [28] as a function of the transverse momentum of a pion in SIDIS in JLab12 kinematics at $x = 0.3$ and $z = 0.3$. Right panel: The same for the $\cos 2\phi$ moments generated by radiative effects.

for $\cos(\phi_h)$ and $\cos(2\phi_h)$ do not appear in Radgen. Therefore, a correct cross-section of the radiated photon cannot be reconstructed using Radgen.

Preliminary analyses (based on HAPRAD 2.0 and SIRAD) are: i) x and Q^2 dependences are similar to what we have in DIS; ii) RC goes down with increasing z, $e.g.$, the RC factor can change from 1.05 to 0.85 between $z = 0.2$ and 0.8 for the same x and Q^2; the z dependence of RC is generated by decreasing the phase space of the radiated photon with increasing z; iii) the P_{hT} dependence is strong: RC can increase by a factor of 2 or more for very high P_{hT}: both semi-inclusive and exclusive processes have large RC for large P_{hT}; iv) RC to ϕ dependence can be large (RC generates new ϕ dependence and therefore new observables like $\langle\cos(3\phi_h)\rangle$ that are exactly zero in SIDIS); and v) RC from exclusive radiative tail has its own dependence on kinematical variables and can give a high contribution especially as small missing mass of the $e'\pi X$, M_x^2 ($e.g.$, 0.95 and 1.4 without and with exclusive radiative tail for $M_x^2 = 1.5\,\mathrm{GeV}^2$ or 1.05 and 1.3 for $M_x^2 = 3.0\,\mathrm{GeV}^2$) and for high P_{hT}. Radiative corrections in the polarized case are largely unknown. The effect in SIDIS may be significant with a strong dependence on the model for structure functions. The strong model dependence can be partly addressed within the RC iteration procedure of the experimental data. An illustration of possible effects of RC in the unpolarized case shows that terms from SFs $F_{UU}^{\cos\phi}$ and $F_{UU}^{\cos 2\phi}$ can significantly contribute to the base term, so higher harmonics generated by RC may be essential. For example, for the kinematical point $E_{\mathrm{beam}} = 10\,\mathrm{GeV}$, $Q^2 = 2.5\,\mathrm{GeV}^2$, $x = 0.25$, $z = 0.2$, and $P_{hT} = 0.7\,\mathrm{GeV}$, the estimate of $\langle\cos 3\phi_h\rangle$ is about 5%, and corrections to the calculated ϕ_h-integrated cross-section only due to presence of ϕ-dependent SFs varies from 3% to 30% depending on different assumptions. Some results obtained from the program HAPRAD [28], specifically developed to calculate the radiative corrections in SIDIS, are presented in fig. 41. Radiative moments can be large at large values of P_{hT} and, in addition some new moments can be generated due to radiative effects. A self-consistent methodology of extraction of TMDs in SIDIS has yet to be developed. The strategy of RC can be developed by generalizing the RC procedure for DIS. The RC procedure of experimental data should involve an iteration procedure in which the fits of SFs of
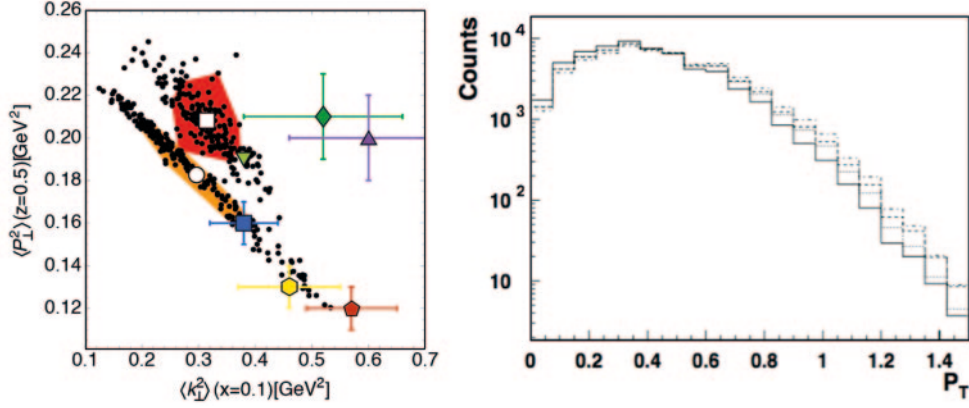
Fig. 42. – Extraction of average P_{hT} and k_T from experiments [51], and variations of the P_{hT} distributions for 4 different combinations of P_{hT} and k_T ($\langle k_T^2 \rangle / \langle P_{hT}^2 \rangle$ = $0.2/0.20, 0.2/0.24, 0.4/0.16, 0.4/0.2\,\mathrm{GeV}^2$) at CLAS12 kinematics for the z bin around 0.5.

interest are re-estimated at each step of this iteration procedure. This procedure could be defined with and without involving Monte Carlo generator. Independently of whether MC is involved, the procedure has to include the following steps: i) the fits of SFs are constructed to have the model in the region covered by the experiment; ii) constructing the models in the regions of softer processes, resonance region, and exclusive scattering using experimental data or theoretical models, iii) checking that the constructed models provide a correct asymptotic behavior when we go to the kinematical bounds (Regge limit, QCD limit); iv) joining all the models to have a continuous function of all four variables in all kinematical regions necessary for RC calculation; v) implementing this scheme in a computer code and define the iteration procedure; vi) implementing the procedure of separation SFs in data and model each of them if several SFs are measured in an experiment; vii) constructing the models for other SFs if necessary (*e.g.*, unpolarized SFs when spin asymmetries are measured); viii) paying specific attention to exclusive SFs, because the radiative tail from exclusive peak is important (or even dominate) in certain kinematical regions; and ix) paying specific attention to P_{hT} dependence, because RC is too sensitive for P_{hT} model choice.

7˙2. *Possible effects due to experimental errors.* – Traditionally SIDIS experiments in most cases extracted different azimuthal moments with the assumption, supported by simplified tests, that other moments in the cross-section have a negligible effect on the moments of interest. Studies of transverse momentum distributions using the SIDIS multiplicities [51] indicate a wide spread of the values for average transverse momentum of quarks due to variation of experimental errors withing few percent (fig. 42). Better separation of different options require wide range in P_{hT}, in particular large P_{hT}, where the experimental acceptances become more complicated, radiative corrections large and cross-sections drop. Unaccounted contributions from higher twists, target mass corrections, target fragmentation, modeling, and other factors, may introduce more significant variations of extracted TMDs, making the validation process crucial.

7˙3. *Energy of the beam and phase space limitations*. – One of the important items in the interpretation of precision data expected from JLab are the phase space limitations due to finite beam energies of real experiments [156]. The cosine modulation in particular is most sensitive to transverse momentum distributions leading to significant corrections due to limitation of the phase space in experiments.

Our studies using MC simulation of Cahn and Boer-Mulders contributions, assuming Gaussian distributions from ref. [156], indicate that phase space limitations may have very different effects on different contributions. Detailed simulations of the effects of accounting for the maximum possible transverse momentum of quarks (assuming on-shell quarks) on the magnitude of the $\cos\phi_h$-moment from two competing contributions suggest that azimuthal moments from different sources can change significantly due to the limited phase space, which suppresses the Cahn contribution [156], and can lead to a relative enhancement of the Boer-Mulders contribution. If the underlying assumptions could be validated, that will indicate a significant suppression of the azimuthal asymmetries generated at the distribution level.

7˙4. *Extraction framework: assumptions and modeling*. – Recent studies have shown that especially in the region of large x, where little or no direct experimental information is available, the uncertainty related to the choice of parametrization and methodology may be as large as or larger than the statistical uncertainty [246, 247]. Various assumptions involved in modern extractions of TMDs from available data rely on conjectures, in particular, on the transverse momentum dependence of distribution and fragmentation functions [248-250, 125, 251-256, 51] making estimates of systematic errors due to those assumptions extremely challenging.

The main goal of the Extraction and VAlidation framework (EVA) is to assist extraction of 3D PDFs, by testing different extraction procedures and estimating systematics related to different assumptions and models used in the extraction procedure [257]. The input of the extraction and validation framework will include also multiplicities and asymmetries, but the preferred input will be the table with Elementary Bin Counts (EBC). The EBC table will contain counts in the smallest size multidimensional bins limited only by detector resolution in all relevant kinematical variables involved in a given process. For example the single-hadron SIDIS will have bins in x, y, z, P_{hT}, ϕ and the exclusive production of photons or mesons, respectively x, y, t, ϕ. The values of helicities for the incoming lepton, λ, and target nucleon, Λ, as well as other relevant information like beam energy, target type, etc., should also be in the table. The counts should be corrected for acceptance, background and other experimental factors, with corresponding statistical and systematic uncertainties. Optionally the radiative correction factor, extracted from unfolding using some specific procedure, could be specified. The resolution size EBC bins would also allow the application of alternative data analysis, typically based on event-by-event procedures (for example, the Bessel-Weighting method [66]).

The EBC table will have info on boundaries of bins and average values of kinematical variables within the elementary bin. The simplest implementation of the EBC file could be by using JavaScript Object Notation (JSON) file format used for serializing and transmitting structured data. A table of values of normalized counts in elementary bins has been extracted in 5-dimensional bins in x, Q^2, z, P_{hT} and ϕ [70]. Full 5-dimensional table with counts in elementary bins with all relevant information (helicities, beam energies, target, . . .) would allow rebinning, proper integrations over other variables, web browsing and graphical presentations. While keeping it human readable, the data will be
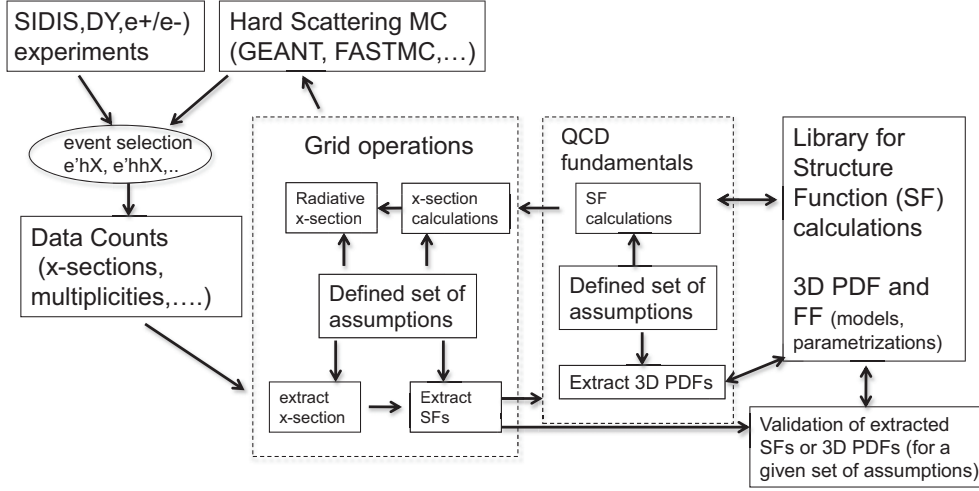
Fig. 43. – The diagram for the extraction and validation framework (EVA).

machine readable (API is needed). The reduction of the size of the bins will be only limited by detector resolution and available MC statistics for acceptance extraction chain. The small size of the bins would allow precision calculations of all relevant variables. Much wider bins, used in experiments, when azimuthal moments were extracted in the process of experimental analysis of the collected data, will always lose some relevant information, limiting the usage of data to specific tasks. More complex processes (like 2 hadron production) will have more variables.

The main challenge in extraction of ϕ_h distributions of hadrons in SIDIS is the handling of the detector acceptance, both geometrical acceptance (the location of active detector elements) and the efficiency in the active regions. For a given kinematical bin, the acceptance is defined as the ratio of the number of reconstructed events (using a GEANT based simulation of the given detector) to the number of generated events.

The overall design of the extraction and validation framework with definitions of the services and data flow between them is shown in fig. 43. The extraction part will take as input the EBC tables and extract SFs based on a given set of SFs from the existing library with radiative corrections applied using the same set. The extracted structure functions will be used to extract underlying TMD PDFs and FFs involved in the calculation of corresponding SFs. The validation process will start with the calculation of relevant (for a given observable) SFs using TMD PDFs and FFs from the library. Those SFs will be used to calculate the Born cross-section, which will be used to calculate the radiative cross-section. The radiative cross-section will be used to generate the process of interest ($e.g.\ ep \to e'\pi^+ X$). The generated events will go through the GEANT simulation and reconstruction chain of a given experiment, eventually providing the EBC table for a given process. The TMD PDFs and FFs extracted from the EBC tables will be compared with input values to validate the process of extraction. The EVA chain would allow estimates of systematic errors due to different assumptions (for instance extraction of the Sivers TMD, ignoring the $\cos \phi_h$ modulation of unpolarized cross-section or SF with $\sin \phi_S$, or ignoring the evolution of 3D PDFs in extraction, and so on). All data flow between different blocks could go through JSON files.

Compared to PDFs, the status of TMD extractions is still in an early stage of development. Phenomenological efforts have been summarized recently by the introduction of a library of fits and parametrizations for transverse-momentum-dependent parton distribution functions (TMD PDFs) and fragmentation functions (TMD FFs) together with an online plotting tool, TMDplotter [243]. Observables constructed by taking ratios, such as asymmetries, are not ideal grounds for the study of TMD evolution effects. More effort should be made towards measuring properly normalized SIDIS and e^+e^-, and Drell-Yan cross-sections (both unpolarized and polarized).

8. – Summary

In summary, spin and azimuthal moments, which may be related to quark-gluon correlations have been measured for all pion channels in a fully differential way and shown to be very significant and flavor dependent. They are an indispensable part of the SIDIS analysis, and their understanding is important for the interpretation of all kinds of spin-azimuthal asymmetries. Comparison of azimuthal moments measured at Jefferson Lab with HERMES and COMPASS measurements supports the higher-twist nature of the $\cos\phi_h$ and $\sin\phi_h$ moments. Measurements of di-hadron single spin asymmetries indicate that the final-state hadrons tend to be correlated. Several effects, including limited phase space for finite beam energies, higher-twist contributions, radiative corrections and possible background from target fragmentation region should be considered as important elements for the interpretation of systematic uncertainties in precision measurements in polarized SIDIS experiments, and in particular at Jefferson Lab. Understanding the scale of contributions ($\sim M^2/Q^2$, $\sim P_{hT}^2/Q^2$, Target/Current correlations, etc.) will define the limits on precision needed to various aspects of TMDs, such as evolution, higher twists, etc. Sophisticated frameworks for the calculation of 3D PDFs, such as TMDlib [243] can be interfaced to extend the scope of available models, which can be used in the validation of 3D PDFs extraction framework. The future Extraction and VAlidation framework will serve to help both the experimental community and the phenomenological community to test results and assure model independence of measured data.

In this review we have not covered hadron-hadron facilities such as RHIC [258], and e^+e^- facilities, such as BELLE. It is however important to emphasize that hadron structure and TMDs in particular are to be studied in as many processes as possible. For instance, measurements in one process, such as SIDIS, cannot definitely answer a question on universality of TMDs. Only a comprehensive study of data coming from various experiments and various processes will allow to unravel the underlying parton landscape of the nucleon.

$$* * *$$

REFERENCES

[1] PROKUDIN A., *Phys. Part. Nucl.*, **44** (2013) 947.
[2] DUDEK J. *et al.*, *Eur. Phys. J. A*, **48** (2012) 187.
[3] ACCARDI A. *et al.*, *Eur. Phys. J. A*, **52** (2016) 268.
[4] ASCHENAUER E.-C. *et al.*, *Eur. Phys. J. A*, **53** (2017) 71.
[5] ABEYRATNE S. *et al.*, arXiv:1209.0757 (2012).
[6] ACCARDI A., GUZEY V., PROKUDIN A. and WEISS C., *Eur. Phys. J. A*, **48** (2012) 92.
[7] ANSELMINO M. *et al.*, *Eur. Phys. J. A*, **47** (2011) 35.
[8] BURKARDT M., *Phys. Rev. D*, **62** (2000) 071503 (Erratum: *Phys. Rev. D*, **66** (2002) 119903).
[9] KOTZINIAN A., *Nucl. Phys. B*, **441** (1995) 234.
[10] MULDERS P. J. and TANGERMAN R. D., *Nucl. Phys. B*, **461** (1996) 197.
[11] BACCHETTA A. *et al.*, *JHEP*, **02** (2007) 093.
[12] METZ A. and VOSSEN A., *Prog. Part. Nucl. Phys.*, **91** (2016) 136.
[13] JAFFE R. L., *Spin, twist and hadron structure in deep inelastic processes*, in *The spin structure of the nucleon. Proceedings of the International School of Nucleon Structure, 1st Course, Erice, Italy, August 3-10, 1995* (World Scientific) 1996, pp. 42–129.
[14] JAFFE R. L., *Comm. Nucl. Part. Phys.*, **19** (1990) 239.
[15] GAMBERG L. P., HWANG D. S., METZ A. and SCHLEGEL M., *Phys. Lett. B*, **639** (2006) 508.
[16] BACCHETTA A., BOER D., DIEHL M. and MULDERS P. J., *JHEP*, **08** (2008) 023.
[17] CHEN K.-B., WEI S.-Y. and LIANG Z.-T., *Front. Phys. (Beijing)*, **10** (2015) 101204.
[18] BOER D. and MULDERS P. J., *Phys. Rev. D*, **57** (1998) 5780.
[19] COLLINS J. C., *Nucl. Phys. B*, **396** (1993) 161.
[20] ALBERG M. and MILLER G. A., arXiv:1712.05814 (2017).
[21] AMAUDRUZ P. *et al.*, *Phys. Rev. Lett.*, **66** (1991) 2712.
[22] GARVEY G. T. and PENG J.-C., *Prog. Part. Nucl. Phys.*, **47** (2001) 203.
[23] NAGAI K., *JPS Conf. Proc.*, **13** (2017) 020051.
[24] COLLINS J., *Foundations of perturbative QCD* (Cambridge University Press) 2013.
URL http://www.cambridge.org/de/knowledge/isbn/item5756723
[25] CAHN R. N., *Phys. Lett. B*, **78** (1978) 269.
[26] BERGER E. L., *Z. Phys. C*, **4** (1980) 289.
[27] AKUSHEVICH I., SHUMEIKO N. and SOROKO A., *Eur. Phys. J. C*, **10** (1999) 681.
[28] AKUSHEVICH I., ILYICHEV A. and OSIPENKO M., *Phys. Lett. B*, **672** (2009) 35.
[29] AKUSHEVICH I., BOTTCHER H. and RYCKBOSCH D., *RADGEN 1.0: Monte Carlo generator for radiative events in DIS on polarized and unpolarized targets*, in *Proceedings of the Workshop Monte Carlo generators for HERA physics, Hamburg, Germany, 1998-1999* (DESY) 1998, pp. 554–565.
URL http://alice.cern.ch/format/showfull?sysnb=0317130
[30] SJOSTRAND T., MRENNA S. and SKANDS P. Z., *JHEP*, **0605** (2006) 026.
[31] INGELMAN G., EDIN A. and RATHSMAN J., *Comput. Phys. Commun.*, **101** (1997) 108.
[32] MANKIEWICZ L., SCHAFER A. and VELTRI M., *Comput. Phys. Commun.*, **71** (1992) 305.
[33] PILAT F. *et al.*, JLEIC Current Design Parameters Short Description (2017).
[34] AUGSTEN K. *et al.*, SPSC-P-340-ADD-1, CERN-SPSC-2017-034 (2017).
[35] ENT R. *et al.*, JLab Experiment E12-06-104 (2006).
[36] ENT R. *et al.*, JLab Experiment E12-09-017 (2009).
[37] ENT R. *et al.*, JLab Experiment E12-09-017 (2013).
[38] CATES G., CISBANI E., FRANKLIN G., PUCKETT A. and B. W., JLab Experiment E12-09-018 (2009).
[39] GAO H., QIAN X. and PENG J.-C., JLab Experiment E12-11-007 (2008).
[40] CHEN J.-P., HUANG J., QIANG Y. and WENBIAO Y., JLab Experiment E12-11-007 (2008).
[41] AVAKIAN H. *et al.*, JLab Experiment E12-06-112 (2006).
[42] AVAKIAN H. *et al.*, JLab Experiment E12-07-107 (2007).

[43] AVAKIAN H. *et al.*, JLab Experiment E12-09-008 (2009).
[44] AVAKIAN H. *et al.*, JLab Experiment E12-09-009 (2009).
[45] AVAKIAN H., JLab LoI LOI-12-14-004 (2014).
[46] BROOKS W. and KUHN S., JLab Experiment E12-14-001 (2014).
[47] SIVERS D. W., *Phys. Rev. D*, **41** (1990) 83.
[48] BOGLIONE M. and PROKUDIN A., *Eur. Phys. J. A*, **52** (2016) 154.
[49] JI X., MA J. and YUAN F., *Phys. Rev. D*, **71** (2005) 034005.
[50] ANSELMINO M., BOGLIONE M., GONZALEZ H. J., MELIS S. and PROKUDIN A., *JHEP*, **1404** (2014) 005.
[51] SIGNORI A., BACCHETTA A., RADICI M. and SCHNELL G., *JHEP*, **1311** (2013) 194.
[52] PASQUINI B., CAZZANIGA S. and BOFFI S., *Phys. Rev. D*, **78** (2008) 034025.
[53] LU Z. and MA B.-Q., *Nucl. Phys. A*, **741** (2004) 200.
[54] ANSELMINO M., EFREMOV A., KOTZINIAN A. and PARSAMYAN B., *Phys. Rev. D*, **74** (2006) 074015.
[55] BOURRELY C., BUCCELLA F. and SOFFER J., *Phys. Rev. D*, **83** (2011) 074008.
[56] HAGLER P., MUSCH B. U., NEGELE J. W. and SCHAFER A., *Europhys. Lett.*, **88** (2009) 61001.
[57] MUSCH B. U., HAGLER P., NEGELE J. W. and SCHAFER A., *Phys. Rev. D*, **83** (2011) 094507.
[58] WAKAMATSU M., *Phys. Rev. D*, **79** (2009) 094028.
[59] SCHWEITZER P., STRIKMAN M. and WEISS C., *JHEP*, **1301** (2013) 163.
[60] BACCHETTA A., DELCARRO F., PISANO C., RADICI M. and SIGNORI A., *JHEP*, **06** (2017) 081.
[61] MATEVOSYAN H. H., BENTZ W., CLOET I. C. and THOMAS A. W., *Phys. Rev. D*, **85** (2012) 014021.
[62] MKRTCHYAN H. *et al.*, *Phys. Lett. B*, **665** (2008) 20.
[63] AIRAPETIAN A. *et al.*, *Phys. Rev. D*, **87** (2013) 074029.
[64] ADOLPH C. *et al.*, *Eur. Phys. J. C*, **73** (2013) 2531.
[65] AGHASYAN M. *et al.*, *Phys. Rev. D*, **97** (2018) 032006.
[66] AGHASYAN M., AVAKIAN H., DE SANCTIS E., GAMBERG L., MIRAZITA M., MUSCH B., PROKUDIN A. and ROSSI P., *JHEP*, **03** (2015) 039.
[67] AKHUNZYANOV R. *et al.*, arXiv:1802.00584 (2018).
[68] ASATURYAN R., ENT R., MKRTCHYAN H., NAVASARDYAN T. and TADEVOSYAN V. *et al.*, *Phys. Rev. C*, **85** (2012) 015202.
[69] AIRAPETIAN A. *et al.*, *Phys. Rev. D*, **87** (2013) 012010.
[70] HARRISON N., AVAKIAN H. and JOO K., *PoS*, DIS2016 (2016) 215.
[71] AIRAPETIAN A. *et al.*, *Phys. Rev. Lett.*, **84** (2000) 4047.
[72] KOTZINIAN A. M. and MULDERS P. J., *Phys. Rev. D*, **54** (1996) 1229.
[73] TANGERMAN R. D. and MULDERS P. J., *Phys. Rev. D*, **51** (1995) 3357.
[74] BRODSKY S. J. and YUAN F., *Phys. Rev. D*, **74** (2006) 094018.
[75] POBYLITSA P. V., hep-ph/0301236 (2003).
[76] GAMBERG L. P., GOLDSTEIN G. R. and SCHLEGEL M., *Phys. Rev. D*, **77** (2008) 094016.
[77] EFREMOV A. V., GOEKE K. and SCHWEITZER P., *Phys. Rev. D*, **67** (2003) 114014.
[78] AVAKIAN H. *et al.*, *Phys. Rev. Lett.*, **105** (2010) 262002.
[79] PARSAMYAN B. (for the COMPASS Collaboration), *PoS*, DIS2017 (2018) 259.
[80] PARSAMYAN B. (for the COMPASS Collaboration), *PoS*, QCDEV2017 (2018) 042.
[81] AVAKIAN H. *et al.*, *Phys. Rev. D*, **77** (2008) 014023.
[82] BASTAMI S. *et al.*, hep-ph/1807.10606 (2018).
[83] JAWALKAR S. *et al.*, *Phys. Lett. B*, **782** (2018) 662.
[84] AIRAPETIAN A. *et al.*, *Phys. Rev. D*, **64** (2001) 097101.
[85] AIRAPETIAN A. *et al.*, *Phys. Lett. B*, **562** (2003) 182.
[86] AIRAPETIAN A. *et al.*, *Phys. Lett. B*, **693** (2010) 11.
[87] ALEXAKHIN V. Y. *et al.*, *Phys. Rev. Lett.*, **94** (2005) 202002.
[88] AGEEV E. S. *et al.*, *Nucl. Phys. B*, **765** (2007) 31.
[89] ALEKSEEV M. *et al.*, *Phys. Lett. B*, **673** (2009) 127.

[90] Adolph C. *et al.*, *Phys. Lett. B*, **717** (2012) 376.
[91] Adolph C. *et al.*, *Phys. Lett. B*, **744** (2015) 250.
[92] Seidl R. *et al.*, *Phys. Rev. D*, **78** (2008) 032011 (Erratum: *Phys. Rev. D*, **86** (2012) 039905).
[93] Anselmino M., Boglione M., D'Alesio U., Kotzinian A., Murgia F. *et al.*, *Phys. Rev. D*, **75** (2007) 054032.
[94] Brodsky S. J., Hwang D. S. and Schmidt I., *Phys. Lett. B*, **530** (2002) 99.
[95] Collins J. C., *Phys. Lett. B*, **536** (2002) 43.
[96] Airapetian A. *et al.*, *Phys. Rev. Lett.*, **94** (2005) 012002.
[97] Alekseev M. G. *et al.*, *Phys. Lett. B*, **692** (2010) 240.
[98] Alekseev M. G. *et al.*, *Eur. Phys. J. C*, **70** (2010) 39.
[99] Adolph C. *et al.*, *Phys. Lett. B*, **713** (2012) 10.
[100] Adolph C. *et al.*, *Phys. Lett. B*, **717** (2012) 383.
[101] Alexeev M. G. *et al.* (for the COMPASS Collaboration), arXiv:1809.02936 [hep-ex] (2018).
[102] Airapetian A. *et al.*, *Phys. Rev. Lett.*, **103** (2009) 152002.
[103] Anselmino M., Boglione M. and Melis S., *Phys. Rev. D*, **86** (2012) 014028.
[104] Aybat S. M., Prokudin A. and Rogers T. C., *Phys. Rev. Lett.*, **108** (2012) 242003.
[105] Echevarria M. G., Idilbi A., Kang Z.-B. and Vitev I., *Phys. Rev. D*, **89** (2014) 074013.
[106] Aybat S. M., Collins J. C., Qiu J.-W. and Rogers T. C., *Phys. Rev. D*, **85** (2012) 034043.
[107] Adolph C. *et al.*, *Phys. Lett. B*, **770** (2017) 138.
[108] Parsamyan B. (for the COMPASS Collaboration), *Int. J. Mod. Phys. Conf. Ser.*, **40** (2016) 1660029.
[109] Parsamyan B. (for the COMPASS Collaboration), *PoS*, QCDEV2015 (2015) 007.
[110] Aybat S. M. and Rogers T. C., *Phys. Rev. D*, **83** (2011) 114042.
[111] Adamczyk L. *et al.*, *Phys. Rev. Lett.*, **116** (2016) 132301.
[112] Aghasyan M. *et al.*, *Phys. Rev. Lett.*, **119** (2017) 112002.
[113] Parsamyan B. (for the COMPASS Collaboration), *PoS*, DIS2017 (2018) 243.
[114] Qian X. *et al.*, *Phys. Rev. Lett.*, **107** (2011) 072003.
[115] Huang J. *et al.*, *Phys. Rev. Lett.*, **108** (2012) 052001.
[116] Zhao Y. X. *et al.*, *Phys. Rev. C*, **90** (2014) 055201.
[117] Zhang Y. *et al.*, *Phys. Rev. C*, **90** (2014) 055209.
[118] Zhao Y. X. *et al.*, *Phys. Rev. C*, **92** (2015) 015207.
[119] Matevosyan H. H., Kotzinian A., Aschenauer E.-C., Avakian H. and Thomas A. W., *Phys. Rev. D*, **92** (2015) 054028.
[120] Ji X. and Yuan F., *Phys. Lett. B*, **543** (2002) 66.
[121] Brodsky S. J., Hwang D. S. and Schmidt I., *Nucl. Phys. B*, **642** (2002) 344.
[122] Bacchetta A., Schaefer A. and Yang J.-J., *Phys. Lett. B*, **578** (2004) 109.
[123] Gamberg L. P., Goldstein G. R. and Oganessyan K. A., *Phys. Rev. D*, **67** (2003) 071504.
[124] Meissner S., Metz A. and Goeke K., *Phys. Rev. D*, **76** (2007) 034002.
[125] Bacchetta A., Gamberg L. P., Goldstein G. R. and Mukherjee A., *Phys. Lett. B*, **659** (2008) 234.
[126] Bacchetta A., Conti F. and Radici M., *Phys. Rev. D*, **78** (2008) 074010.
[127] Gamberg L. P., Mukherjee A. and Mulders P. J., *Phys. Rev. D*, **77** (2008) 114026.
[128] Schweitzer P., Teckentrup T. and Metz A., *Phys. Rev. D*, **81** (2010) 094019.
[129] Avakian H., Efremov A. V., Schweitzer P. and Yuan F., *Phys. Rev. D*, **81** (2010) 074035.
[130] Boffi S. *et al.*, *Phys. Rev. D*, **79** (2009) 094012.
[131] Pasquini B. and Yuan F., *Phys. Rev. D*, **81** (2010) 114013.
[132] Pasquini B. and Schweitzer P., *Phys. Rev. D*, **83** (2011) 114044.
[133] Pasquini B. and Schweitzer P., *Phys. Rev. D*, **90** (2014) 014050.

[134] MUSCH B. U., *Transverse momentum distributions inside the nucleon from lattice QCD*, Ph.D. thesis, Munich, Tech. U. (May 2009).

[135] AIRAPETIAN A. *et al.* (for the HERMES Collaboration), arXiv:1810.07054 [hep-ex] (2018).

[136] KOTZINIAN A., PARSAMYAN B. and PROKUDIN A., *Phys. Rev. D*, **73** (2006) 114017.

[137] PAPPALARDO L. L., *Nuovo Cimento B*, **125** (2010) 51.

[138] AVAKIAN H. *et al.*, JLab Experiment C12-11-111 (2011).

[139] AUBERT J. J. *et al.*, *Phys. Lett. B*, **130** (1983) 118.

[140] ARNEODO M. *et al.*, *Z. Phys. C*, **34** (1987) 277.

[141] AVAKIAN H., *Nucl. Phys. Proc. Suppl.*, **79** (1999) 523.

[142] AVAKIAN H. *et al.*, *Phys. Rev. D*, **69** (2004) 112004.

[143] AGHASYAN M., AVAKIAN H., ROSSI P. and DE SANCTIS E. *et al.*, *Phys. Lett. B*, **704** (2011) 397.

[144] GOHN W. *et al.*, *Phys. Rev. D*, **89** (2014) 072011.

[145] GEORGI H. and POLITZER H. D., *Phys. Rev. Lett.*, **40** (1978) 3.

[146] BURKARDT M., *Spin-Orbit Correlations*, presented at *Transversity 2008: 2nd International Workshop on Transverse Polarization Phenomena in Hard Processes Ferrara, Italy, May 28-31, 2008* (World Scientific) 2008.

[147] WANDZURA S. and WILCZEK F., *Phys. Lett. B*, **72** (1977) 195.

[148] DE SANCTIS E., NOWAK W. D. and OGANESIAN K. A., *Phys. Lett. B*, **483** (2000) 69.

[149] MA B.-Q., SCHMIDT I. and YANG J.-J., *Phys. Rev. D*, **63** (2001) 037501.

[150] EFREMOV A. V., GOEKE K. and SCHWEITZER P., *Phys. Lett. B*, **522** (2001) 37.

[151] ACCARDI A., BACCHETTA A., MELNITCHOUK W. and SCHLEGEL M., *JHEP*, **11** (2009) 093.

[152] ADAMS M. R. *et al.*, *Phys. Rev. D*, **48** (1993) 5057.

[153] BREITWEG J. *et al.*, *Phys. Lett. B*, **481** (2000) 199.

[154] OSIPENKO M. *et al.*, *Phys. Rev. D*, **80** (2009) 032004.

[155] ADOLPH C. *et al.*, *Nucl. Phys. B*, **886** (2014) 1046.

[156] BOGLIONE M., MELIS S. and PROKUDIN A., *Phys. Rev. D*, **84** (2011) 034033.

[157] AIRAPETIAN A. *et al.*, *Phys. Lett. B*, **622** (2005) 14.

[158] MULDERS P. J. and RODRIGUES J., *Quark distribution functions in a diquark spectator model*, in *Proceedings of the 3rd Workshop "Diquarks 3", Torino, Italy, October 28-30, 1996* (World Scientific, Singapore) 1998, pp. 208–217.

[159] BACCHETTA A., MULDERS P. J. and PIJLMAN F., *Phys. Lett. B*, **595** (2004) 309.

[160] JAFFE R. L. and JI X.-D., *Nucl. Phys. B*, **375** (1992) 527.

[161] SIGNAL A. I., *Nucl. Phys. B*, **497** (1997) 415.

[162] JAKOB R., MULDERS P. J. and RODRIGUES J., *Nucl. Phys. A*, **626** (1997) 937.

[163] SCHWEITZER P., *Phys. Rev. D*, **67** (2003) 114010.

[164] WAKAMATSU M. and OHNISHI Y., *Phys. Rev. D*, **67** (2003) 114011.

[165] LORCE C., PASQUINI B. and SCHWEITZER P., *JHEP*, **01** (2015) 103.

[166] LU Z. and SCHMIDT I., *Phys. Lett. B*, **747** (2015) 357.

[167] JAFFE R. L., *Nucl. Phys. B*, **229** (1983) 205.

[168] BALLA J., POLYAKOV M. V. and WEISS C., *Nucl. Phys. B*, **510** (1998) 327.

[169] DRESSLER B. and POLYAKOV M. V., *Phys. Rev. D*, **61** (2000) 097501.

[170] WAKAMATSU M., *Phys. Lett. B*, **509** (2001) 59.

[171] OHNISHI Y. and WAKAMATSU M., *Phys. Rev. D*, **69** (2004) 114002.

[172] CEBULLA C., OSSMANN J., SCHWEITZER P. and URBANO D., *Acta Phys. Pol. B*, **39** (2008) 609.

[173] BURKARDT M. and KOIKE Y., *Nucl. Phys. B*, **632** (2002) 311.

[174] MUKHERJEE A., *Phys. Lett. B*, **687** (2010) 180.

[175] SCHWEITZER P. *et al.*, *Phys. Rev. D*, **64** (2001) 034013.

[176] TANGERMAN R. D. and MULDERS P. J., hep-ph/9408305 (1994).

[177] METZ A., SCHWEITZER P. and TECKENTRUP T., *Phys. Lett. B*, **680** (2009) 141.

[178] PASQUINI B. and RODINI S., arXiv:1806.10932 (2018).

[179] MUSCH B., HAGLER P., ENGELHARDT M., NEGELE J. and SCHAFER A., *Phys. Rev. D*, **85** (2012) 094510.

[180] ENGELHARDT M., HAGLER P., MUSCH B., NEGELE J. and SCHAFER A., *Phys. Rev. D*, **93** (2016) 054501.

[181] ENGELHARDT M., private communications (2018).

[182] KOTSINIAN A. M., OGANESIAN K. A., AVAKIAN H. and DE SANCTIS E., *Nucl. Phys. A*, **666** (2000) 290.

[183] BOGLIONE M. and MULDERS P. J., *Phys. Lett. B*, **478** (2000) 114.

[184] EFREMOV A. V. *et al.*, *Phys. Lett. B*, **478** (2000) 94.

[185] ANSELMINO M. and MURGIA F., *Phys. Lett. B*, **483** (2000) 74.

[186] OGANESSIAN K. A., BIANCHI N., DE SANCTIS E. and NOWAK W. D., *Nucl. Phys. A*, **689** (2001) 784.

[187] EFREMOV A. V., GOEKE K. and SCHWEITZER P., *Eur. Phys. J. C*, **24** (2002) 407.

[188] MA B.-Q., SCHMIDT I. and YANG J.-J., *Phys. Rev. D*, **65** (2002) 034010.

[189] BACCHETTA A., KUNDU R., METZ A. and MULDERS P. J., *Phys. Rev. D*, **65** (2002) 094021.

[190] EFREMOV A. V., GOEKE K. and SCHWEITZER P., *Nucl. Phys. A*, **711** (2002) 84.

[191] MA B.-Q., SCHMIDT I. and YANG J.-J., *Phys. Rev. D*, **66** (2002) 094001.

[192] EFREMOV A. V., GOEKE K. and SCHWEITZER P., *Phys. Lett. B*, **568** (2003) 63.

[193] EFREMOV A. V., GOEKE K. and SCHWEITZER P., *Eur. Phys. J. C*, **32** (2003) 337.

[194] SCHWEITZER P. and BACCHETTA A., *Nucl. Phys. A*, **732** (2004) 106.

[195] EFREMOV A. V., GOEKE K. and SCHWEITZER P., *Czech. J. Phys.*, **55** (2005) A189.

[196] AFANASEV A. and CARLSON C. E., *Single spin beam asymmetry in semiexclusive deep inelastic electroproduction*, presented at *Intersections of particle and nuclear physics. Proceedings of the 8th Conference CIPANP 2003, New York, USA, May 19-24, 2003* URL http://www1.jlab.org/Ul/publications/view_pub.cfm?pub_id=4996

[197] YUAN F., *Phys. Lett. B*, **589** (2004) 28.

[198] METZ A. and SCHLEGEL M., *Eur. Phys. J. A*, **22** (2004) 489.

[199] JI X.-D., *Phys. Rev. D*, **49** (1994) 114.

[200] LEVELT J. and MULDERS P. J., *Phys. Lett. B*, **338** (1994) 357.

[201] OGANESIAN K. A., AVAKIAN H. R., BIANCHI N. and DI NEZZA P., *Eur. Phys. J. C*, **5** (1998) 681.

[202] PARSAMYAN B. (for the COMPASS Collaboration), *Eur. Phys. J. ST*, **162** (2008) 89.

[203] AIRAPETIAN A. *et al.*, *Phys. Lett. B*, **648** (2007) 164.

[204] MARUKYAN H., *J. Phys. Conf. Ser.*, **938** (2017) 012011.

[205] MAO W. and LU Z., *Phys. Rev. D*, **87** (2013) 014012.

[206] LU Z. and MAO W., *Int. J. Mod. Phys. Conf. Ser.*, **40** (2016) 1660045.

[207] OGANESSIAN K. A., AVAKIAN H. R., BIANCHI N. and KOTZINIAN A. M., *Sin(phi) azimuthal asymmetry in semiinclusive electroproduction on longitudinally polarized nucleon, The structure of baryons. Proceedings of the 8th International Conference "Baryons'98", Bonn, Germany, September 22-26, 1998* (World Scientific Pub Co Inc) 1998 edition, pp. 320–324.

[208] AVAKIAN H. *et al.*, JLab Experiment E12-06-015 (2008).

[209] MAO W., WANG X., DU X., LU Z. and MA B.-Q., *Nucl. Phys. A*, **945** (2016) 153.

[210] AFANASEV A., CARLSON C. E. and WAHLQUIST C., *Phys. Lett. B*, **398** (1997) 393.

[211] ABE K. *et al.*, *Phys. Rev. Lett.*, **96** (2006) 232002.

[212] LEES J. P. *et al.*, *Phys. Rev. D*, **90** (2014) 052003.

[213] ABLIKIM M. *et al.*, *Phys. Rev. Lett.*, **116** (2016) 042001.

[214] DEFURNE M. *et al.*, *Phys. Rev. Lett.*, **117** (2016) 262001.

[215] ARTRU X. and MEKHFI M., *Z. Phys. C*, **45** (1990) 669.

[216] RADICI M. and BACCHETTA A., *Phys. Rev. Lett.*, **120** (2018) 192001.

[217] BOER D., JAKOB R. and MULDERS P. J., *Nucl. Phys. B*, **504** (1997) 345.

[218] LEES J. P. *et al.*, *Phys. Rev. D*, **90** (2014) 052003.

[219] COLLINS J. C. and SOPER D. E., *Nucl. Phys. B*, **193** (1981) 381.

[220] BOER D., *Nucl. Phys. B*, **806** (2009) 23.

[221] BOER D., GAMBERG L., MUSCH B. and PROKUDIN A., *JHEP*, **1110** (2011) 021.

[222] KANG Z.-B., PROKUDIN A., SUN P. and YUAN F., *Phys. Rev. D*, **91** (2015) 071501.

[223] KANG Z.-B., PROKUDIN A., SUN P. and YUAN F., *Phys. Rev. D*, **93** (2016) 014009.

[224] ANSELMINO M., BOGLIONE M., D'ALESIO U., KOTZINIAN A., MURGIA F., PROKUDIN A. and MELIS S., *Nucl. Phys. Proc. Suppl.*, **191** (2009) 98.

[225] COLLINS J. C., SOPER D. E. and STERMAN G., *Adv. Ser. Direct. High Energy Phys.*, **5** (1988) 1.

[226] BROCK R. *et al.*, *Rev. Mod. Phys.*, **67** (1995) 157.

[227] LIN H.-W., MELNITCHOUK W., PROKUDIN A., SATO N. and SHOWS H., *Phys. Rev. Lett.*, **120** (2018) 152502.

[228] AIRAPETIAN A. *et al.*, *Phys. Lett. B*, **442** (1998) 484.

[229] PROK Y. *et al.*, *Phys. Rev. C*, **90** (2014) 025212.

[230] ABE K. *et al.*, *Phys. Rev. Lett.*, **74** (1995) 346.

[231] ANTHONY P. L. *et al.*, *Phys. Lett. B*, **493** (2000) 19.

[232] ADOLPH C. *et al.*, *Phys. Lett. B*, **753** (2016) 406.

[233] AVAKIAN H. *et al.*, JLab Experiment C12-12-009 (2012).

[234] GAO H., CHEN J.-P., XIAO Z. and COURTOY A., JLab Experiment E12-10-006A (2008).

[235] CZYZEWSKI J., *Acta Phys. Pol.*, **27** (1996) 1759.

[236] AVAKIAN H. and ELOUADRHIRI L., *Single spin asymmetries in electroproduction at CLAS*, in *Gerasimov-Drell-Hearn sum rule and its extensions. Proceedings of the 3rd International Symposium, GDH 2004, Norfolk, USA, June 2-5, 2004* (World Scientific, New Jersey) 2005, pp. 228–232
URL http://www1.jlab.org/Ul/publications/view_pub.cfm?pub_id=6599

[237] BACCHETTA A. and RADICI M., *Phys. Rev. D*, **69** (2004) 074026.

[238] MATEVOSYAN H. H., arXiv:1807.11485 (2018).

[239] MATEVOSYAN H. H., KOTZINIAN A. and THOMAS A. W., *Phys. Rev. Lett.*, **120** (2018) 252001.

[240] ANSELMINO M., BARONE V. and KOTZINIAN A., *Phys. Lett. B*, **706** (2011) 46.

[241] PISANO S., *EPJ Web of Conferences*, **73** (2014) 02008.

[242] AVAKIAN H. and PISANO S., *PoS*, DIS2016 (2016) 214.

[243] HAUTMANN F., JUNG H., KRAMER M., MULDERS P. and NOCERA E. *et al.*, arXiv:1408.3015 (2014).

[244] ALEKHIN S., BEHNKE O., BELOV P., BORRONI S. and BOTJE M. *et al.*, arXiv:1410.4412 (2014).

[245] HAUTMANN F., JUNG H. and MONFARED S. T., *Eur. Phys. J. C*, **74** (2014) 3082.

[246] AARON F. *et al.*, *JHEP*, **1001** (2010) 109.

[247] JIMENEZ-DELGADO P., AVAKIAN H. and MELNITCHOUK W., *Phys. Lett. B*, **738** (2014) 263.

[248] DE FLORIAN D., SASSOT R. and STRATMANN M., *Phys. Rev. D*, **75** (2007) 114010.

[249] ANSELMINO M., BOGLIONE M., D'ALESIO U., KOTZINIAN A., MURGIA F. and PROKUDIN A., *Phys. Rev. D*, **71** (2005) 074006.

[250] AMRATH D., BACCHETTA A. and METZ A., *Phys. Rev. D*, **71** (2005) 114018.

[251] MATEVOSYAN H. H., THOMAS A. W. and BENTZ W., *Phys. Rev. D*, **83** (2011) 074003.

[252] HIRAI M., KUMANO S., NAGAI T.-H. and SUDOH K., *Phys. Rev. D*, **75** (2007) 094009.

[253] ANSELMINO M., BOGLIONE M., D'ALESIO U., KOTZINIAN A., MELIS S. *et al.*, *Eur. Phys. J. A*, **39** (2009) 89.

[254] MATEVOSYAN H. H., THOMAS A. W. and BENTZ W., *Phys. Rev. D*, **86** (2012) 034025.

[255] MATEVOSYAN H. H., BENTZ W., CLOET I. C. and THOMAS A. W., *Phys. Rev. D*, **85** (2012) 014021.

[256] CASEY A., CLOET I. C., MATEVOSYAN H. H. and THOMAS A. W., *Phys. Rev. D*, **86** (2012) 114018.

[257] AVAKIAN H., MATEVOSYAN H., PASQUINI B. and SCHWEITZER P., *J. Phys. G*, **42** (2015) 034015.

[258] ASCHENAUER E.-C. *et al.*, arXiv:1501.01220 (2015).